

**ROCHESTER INSTITUTE OF TECHNOLOGY
MICROELECTRONIC ENGINEERING**

***Microelectromechanical Systems (MEMs)
Applications – Microphones***

Dr. Lynn Fuller

Webpage: <http://people.rit.edu/lffeee>

Microelectronic Engineering
Rochester Institute of Technology

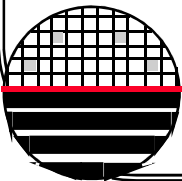
82 Lomb Memorial Drive
Rochester, NY 14623-5604

Tel (585) 475-2035

Fax (585) 475-5041

Email: Lynn.Fuller@rit.edu

Department webpage: <http://www.microe.rit.edu>



OUTLINE

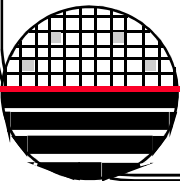
An Integrated Air-Gap-Capacitor Pressure Sensor and Digital Readout with Sub-100 Attofarad Resolution

A Novel Integrated Silicon Capacitive Microphone – Floating Electrode “Electret” Microphone

High-Performance Condenser Microphone with Full Integrated CMOS Amplifier and DC-DC Voltage Converter

A High Sensitivity Polysilicon Diaphragm Condenser Microphone

Commercial Microphones



INTEGRATED CAPACITOR PRESSURE SENSOR

JOURNAL OF MICROELECTROMECHANICAL SYSTEMS, VOL. 1, NO. 3, SEPTEMBER 1992

121

An Integrated Air-Gap-Capacitor Pressure Sensor and Digital Readout with Sub-100 Attifarad Resolution

Joseph T. Kung and Hae-Seung Lee

Abstract—The fabrication and characterization of an integrated air-gap-capacitor pressure sensor is presented. The capacitor fabrication process uses standard IC processing to create NMOS circuits, and an added polysilicon layer to create poly-to- n^+ capacitors with a 0.6- μm -thick dielectric using deposited oxide. Subsequent processing is used to etch the oxide under the polysilicon from the back of the substrate (formed using bulk etching), to produce deformable, parallel-plate, air-gap capacitors on the front-side alongside MOS circuits. Sensor chips are fabricated using $100 \times 100 \mu\text{m}$, 100 fF air-gap capacitors with on-chip circuitry. The sensor chip is a part of a capacitive measurement system that uses a charge-redistribution sense technique to achieve very high capacitance resolution. The pressure sensor chips were characterized versus applied pressure in the 0–240 kPa (0–35 psi) range using optical phase measurement interferometry to measure deflection and shape, and charge-redistribution sense techniques to measure capacitance change. Measurements indicate a sensitivity of 0.93 mV/kPa (6.40 mV/psi) with a deflection of 10 nm/kPa (70 nm/psi) from 0–69 kPa (0–10 psi). Standard deviations indicate a static pressure resolution of 0.54 kPa (0.078 psi), which translates to 30 attofarads at a sampling frequency of 11 kHz.

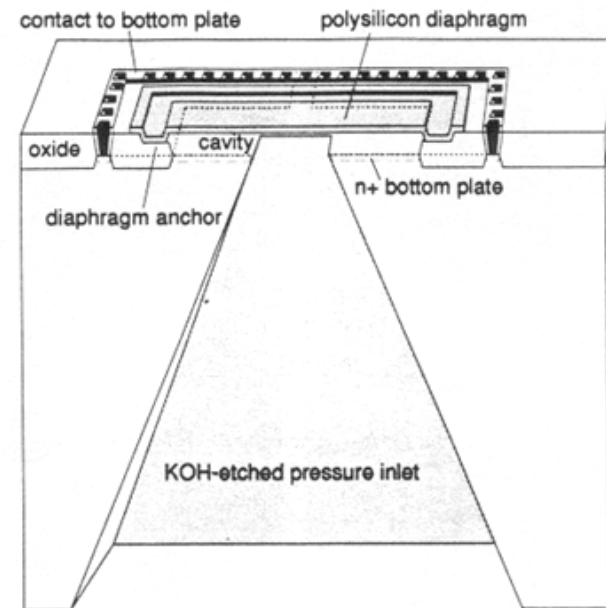
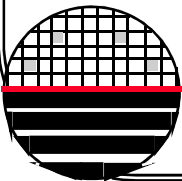


Fig. 1. Air-gap-capacitor structure implemented using an existing MOS process with minor modifications.

INTEGRATED CAPACITOR PRESSURE SENSOR

Introduction

1. States that capacitor detection can be more sensitive than piezoresistive detection and less temperature dependent.
2. States that capacitor structures with small gaps are difficult to make.
3. States that electronic circuits are more complex for capacitor detectors
4. Acknowledges that this design, the maximum deflection of the diaphragm occurs over the hole opening, and gives decreased sensitivity.
5. Fabrication process is compatible with standard IC technology (nMOS or CMOS) and that the MEMs structure (hole, etch of sacrificial layer) is made after standard processing by etching from the backside.



INTEGRATED CAPACITOR PRESSURE SENSOR

4” wafers, 500 μm , (100), p-type, 15 ohm-cm, With nMOS done

Backside polish to mirror finish

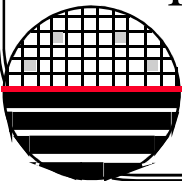
Deposit pad oxide (500 \AA) and nitride (1500 \AA)

Etch pad oxide off back of wafer so nitride deposition goes directly on the back of the wafer and is the hole mask

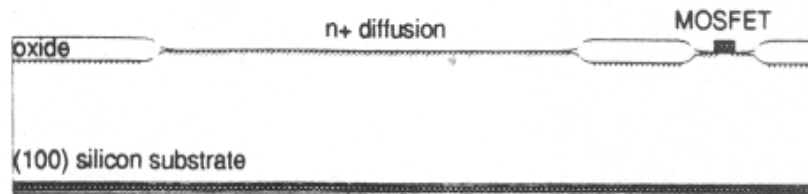
Field oxide is grown for the MOS IC

A low temp (400 C) boro-phospho-silicate glass is deposited and will become the sacrificial layer defining the capacitor air gap, flowed/anneal for step smoothing, and etched down to the nitride to remove everywhere except where capacitors are to be formed

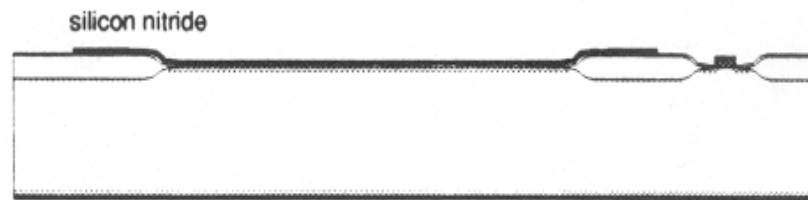
The poly for the MOSFET gate and capacitor top plate is 1 μm



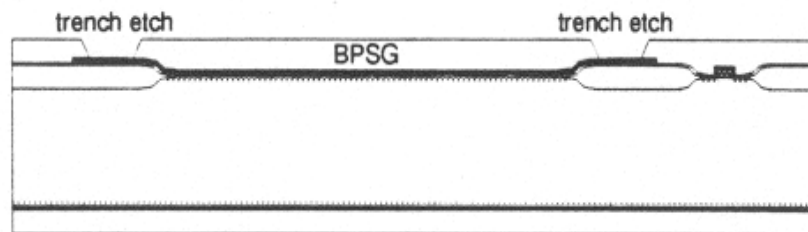
INTEGRATED CAPACITOR PRESSURE SENSOR



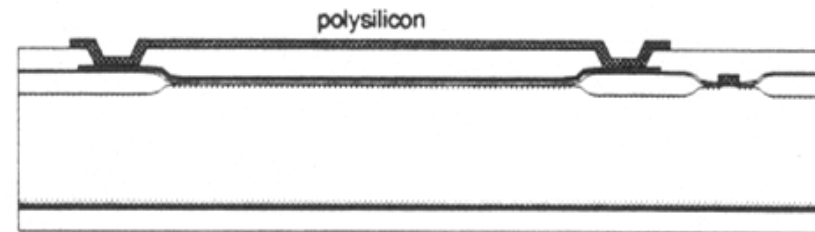
(a)



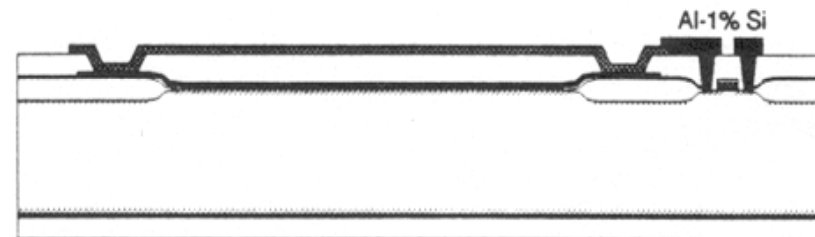
(b)



(c)



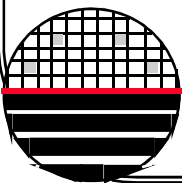
(d)



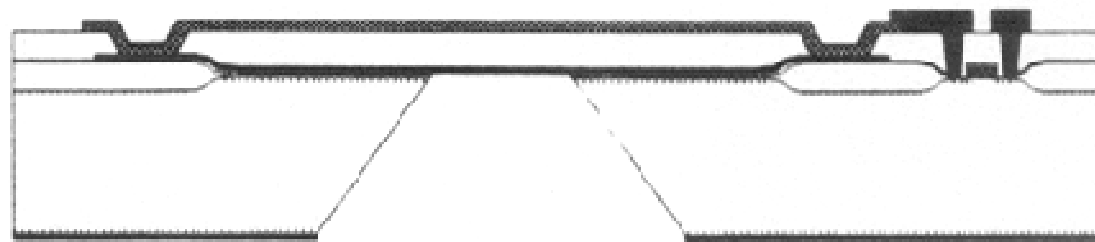
Front-side IC processing completed

(e)

Fig. 2. Front-side process cross section: (a) after NMOS processing up to patterning and etching of the polysilicon gates, reoxidation, and junction drive-in of the source/drain regions; (b) after deposition and patterning of LPCVD silicon nitride layer; (c) after BPSG deposition, flow/anneal, and trench cut for the diaphragm anchor; (d) LPCVD deposition of 1 μm of polysilicon, phosphorus doping, glass wet etch, polysilicon patterning, and etching; (e) after contact cuts, aluminum-1% silicon sputter deposition, and sinter.

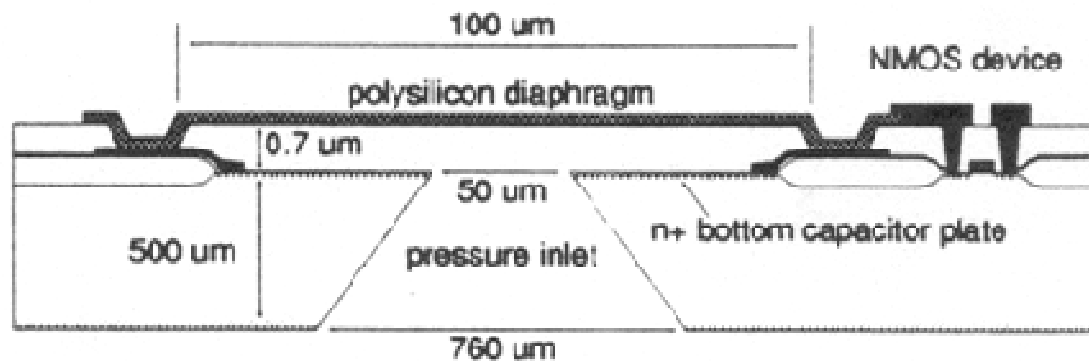


INTEGRATED CAPACITOR PRESSURE SENSOR



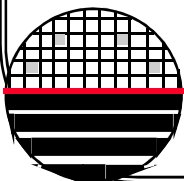
One-sided anisotropic KOH etch : 80 C 6 hours, 60 C 2 hours

(a)



(b)

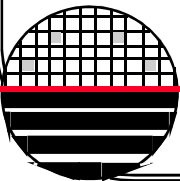
Fig. 3. Backside process cross sections: (a) after IR alignment for back-side nitride patterning/etching, and one-sided KOH etch; (b) after one-sided concentrated HF etch.



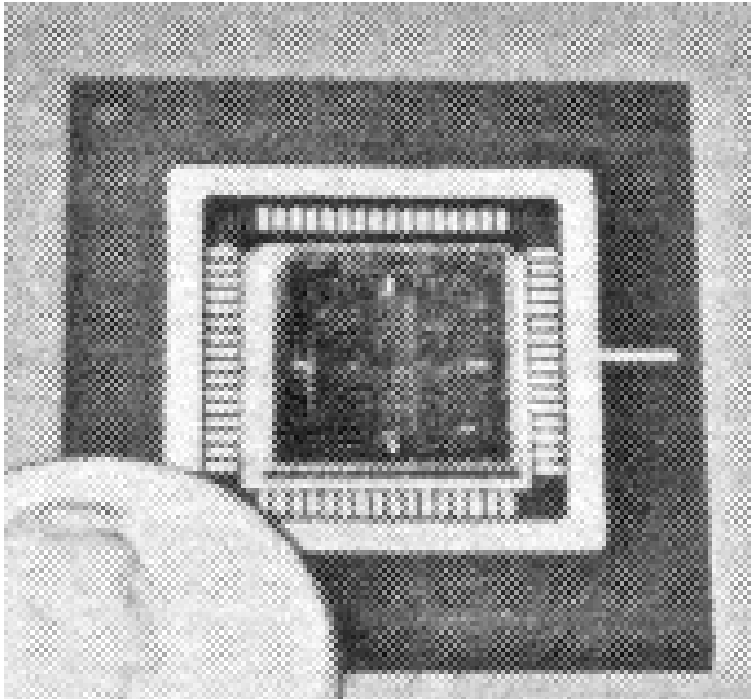
INTEGRATED CAPACITOR PRESSURE SENSOR

TABLE I
KEY PROCESS PARAMETERS IN THE NMOS/AIR-GAP-CAPACITOR
PROCESS

Key Process Parameters	
NMOS threshold voltage	0.7 V
Gate oxide thickness	22 nm
Field oxide thickness	400 nm
Field threshold voltage	> 12 V
Poly gate thickness	500 nm
Dielectric	100 nm LTO, 500 nm BPSG
Metal	Al-1% Si, 1100 nm
n + junction depth	350 nm
Junction breakdown	> 10 V
Poly diaphragm size	100 μm square
Poly diaphragm thickness	1 μm
Air-gap spacing	700 nm



INTEGRATED CAPACITOR PRESSURE SENSOR



Packaged chip with 4 sensors. Holes are drilled into other side and tygon tubing is epoxied into place.

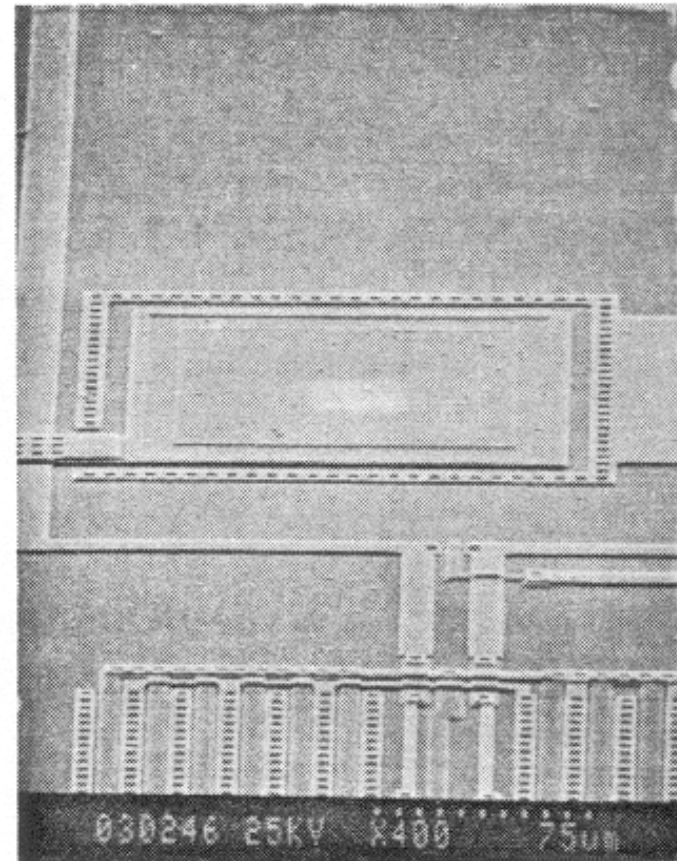
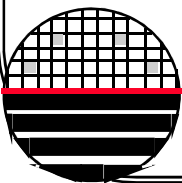


Fig. 5. SEM of an air-gap capacitor after all processing.



INTEGRATED CAPACITOR PRESSURE SENSOR

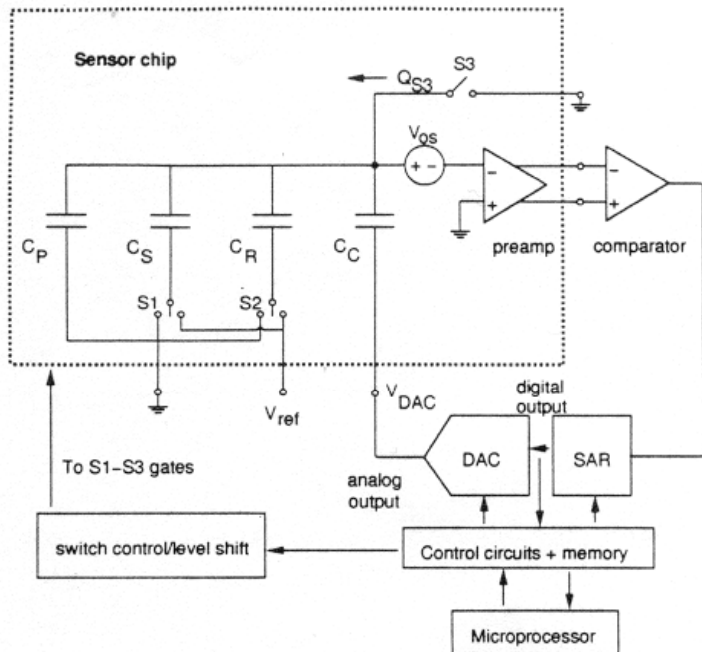


Fig. 6. Capacitance measurement system block diagram.

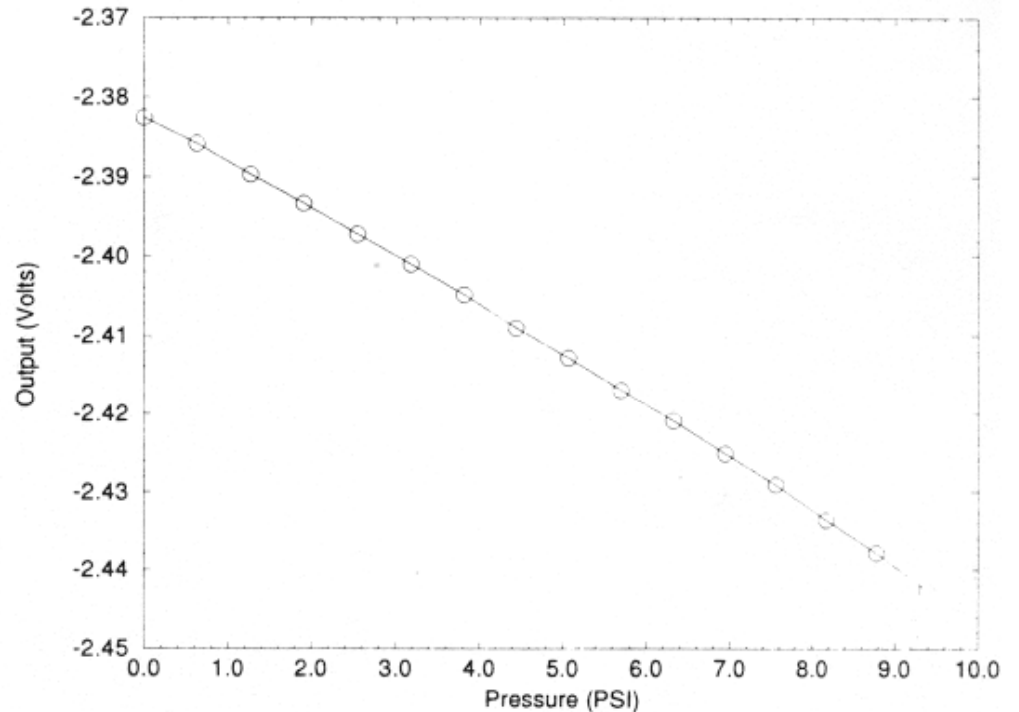
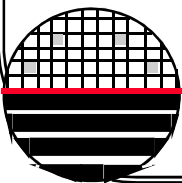


Fig. 7. Measured voltage output versus pressure input for an integrated capacitive pressure sensor. Size of the diaphragm is $100 \times 100 \mu\text{m}$, $1 \mu\text{m}$ thick, with a $60\text{-}\mu\text{m}$ front-side hole opening and a $0.7 \mu\text{m}$ air gap ($1 \text{ psi} = 6.89 \text{ kPa}$).



INTEGRATED CAPACITOR PRESSURE SENSOR

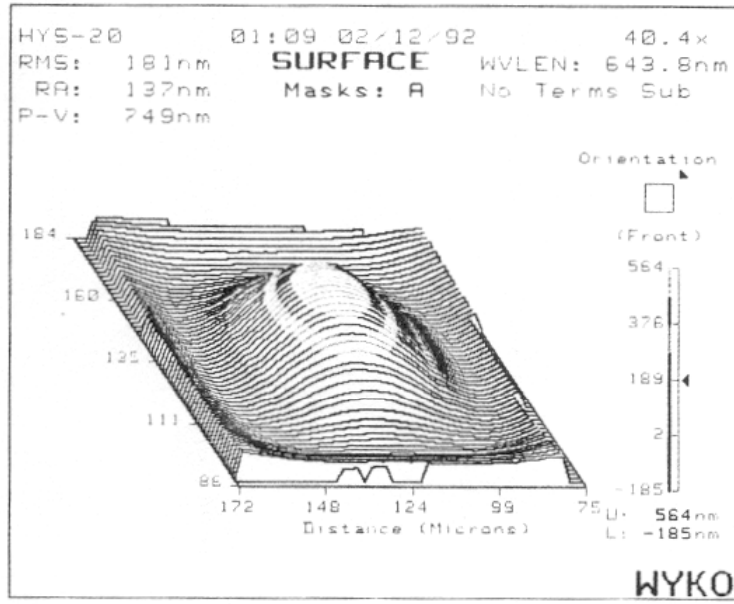


Fig. 11. Measured 3-D surface profile (using PMI) of an air-gap sense capacitor diaphragm: (a) at 11 psi; (b) at 20 psi differential pressure (1 psi = 6.89 kPa).

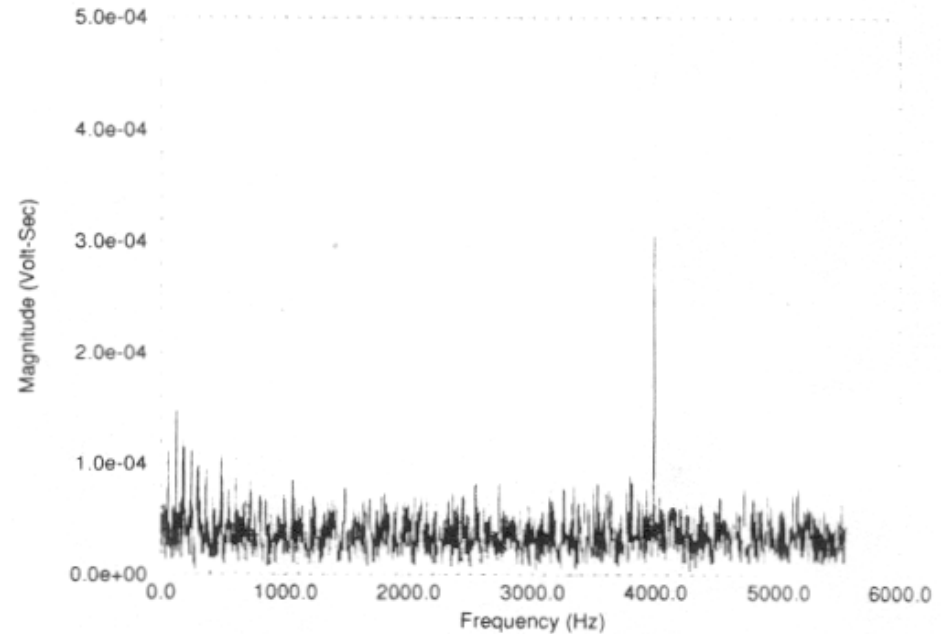
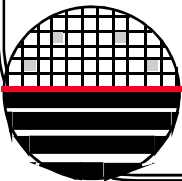


Fig. 12. 4096-point FFT using a rectangular window at a sampling rate of 11.111 kHz for a 4 kHz sine wave input from a sound source at 125-dB SPL.

Deflection measurements using
Phase measurement interferometry

Acoustic Measurements using a loudspeaker

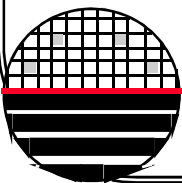


INTEGRATED CAPACITOR PRESSURE SENSOR

V. CONCLUSIONS

The fabrication and characterization of an integrated air-gap-capacitor pressure sensor has been described. The fabrication process combines MOS processing and surface and bulk micromachining in a way that preserves existing MOS device process parameters and allows some optimization of the mechanical design of the diaphragm. Pressure is sensed with a charge redistribution sense capacitance technique that allows high resolution, enabling small sensor capacitors to be used as sense structures, which in turn necessitates some degree of sensor and circuit integration. Air-gap capacitors have been successfully used in a pressure sensor for measurement of differential gas pressure.

The sensors use charge-redistribution sense techniques that demonstrate capacitance-change resolution of less than 30 attofarads in a single measurement without averaging, and two attofarads with averaging. Optical deflection measurements were performed using a phase measurement interferometry surface profiler. This is the first load deflection measurement of this kind on surface micromachined capacitive integrated pressure sensors in the 100-fF range. Deflections in the 20–350-nm range were seen with applied pressure from 0 to 69 kPa (0 to 10 psi). The PMI technique was used to quantify the warped nature of the diaphragm and allow accurate future modeling and simulation. Finally, the PMI technique was able to correlate well with capacitance measurements in the transition region of the diaphragm where it dramatically changes shape. This enabled separate verification that the capacitance change detected by the system was due to deflection of the polysilicon plate by applied pressure. Future improvements in thin-film uniformity and lowering of residual stresses (by rapid thermal annealing or unique deposition conditions) should enable flatter structures with predictable deflection characteristics.



ELECTRET MICROPHONE

224

JOURNAL OF MICROELECTROMECHANICAL SYSTEMS, VOL. 7, NO. 2, JUNE 1998

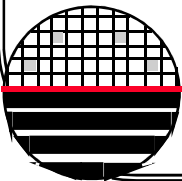
A Novel Integrated Silicon Capacitive Microphone—Floating Electrode “Electret” Microphone (FEEM)

Quanbo Zou, Zhimin Tan, Zhenfeng Wang, Jiangtao Pang, Xin Qian, Qingxin Zhang,
Rongming Lin, Sung Yi, Haiqing Gong, Litian Liu, and Zhijian Li

Abstract—A novel principle “electret” microphone, i.e., floating electrode electret microphone, is proposed and implemented in this study. Single-chip fabrication and corrugation technique are used in the design and fabrication of the microphone. The floating electrode is encapsulated by highly insulated materials to ensure that there is no electric-leakage passage between the floating electrode and the electrodes of the microphone. Net-free electronic charges (not “bonded” charges as in traditional electret) in the floating electrode can excite the electric field, which is similar to that of the traditional electret. The floating electrode can be easily charged by use of the “hot” electron technique, available using the avalanche breakdown of the $p^+ - n$ junction. Therefore, the electret microphone is rechargeable, which can greatly increase the lifetime of the device. The preamplifier has been on-chip

integrated in a junction-field-effect transistor (JFET) source-follower type with resistors by use of ion implantation. Electret charges are bonded in a deep potential trap, thus, this microphone can operate at a high temperature (as high as 300°C) and has high stability and reliability. Experiments show that the prototype has a 3-mV/Pa sensitivity and a larger than 21-kHz frequency bandwidth in a $1\text{ mm} \times 1\text{-mm}$ diaphragm area. Microphone performance can be further improved by optimized process and design. The fabrication is completely integrated-circuit (IC) compatible, hence, the microphone shows promise in integrated acoustic systems. [304]

Index Terms— Corrugated diaphragm, electret microphone, integrated microphone, micromachining, single-chip fabrication.

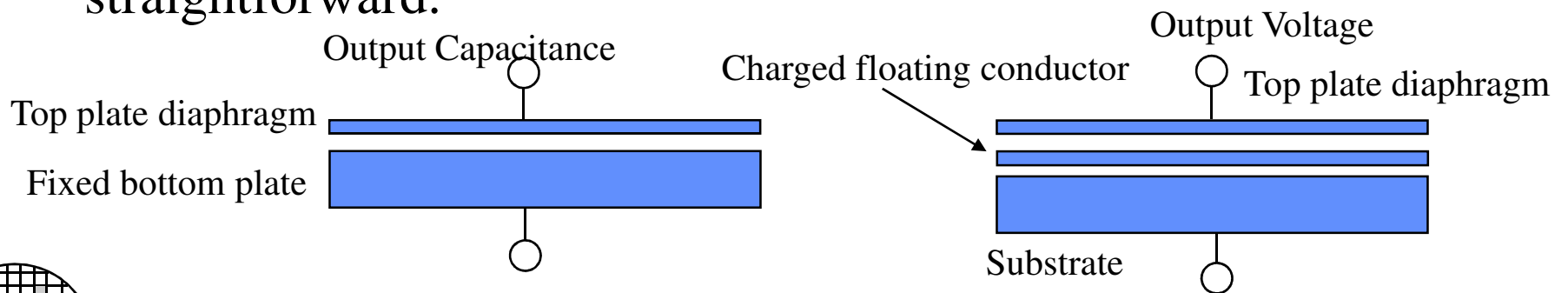


Rochester Institute of Technology
Microelectronic Engineering

ELECTRET MICROPHONE

Introduction

1. States that a condenser microphone requires an external bias voltage for operation, while electret microphone does not.
2. States that electret structures historically used conductors in Teflon FEP which is not compatible with IC/MEMs fabrication. Polysilicon conductors in SiO₂ have shown decay time constants of 400 years in EEPROM applications.
3. States that the fabrication technology described here is superior to other MEMs electret approaches which glue two wafers together.
4. Electrical output signal is voltage making signal processing straightforward.



ELECTRET MICROPHONE

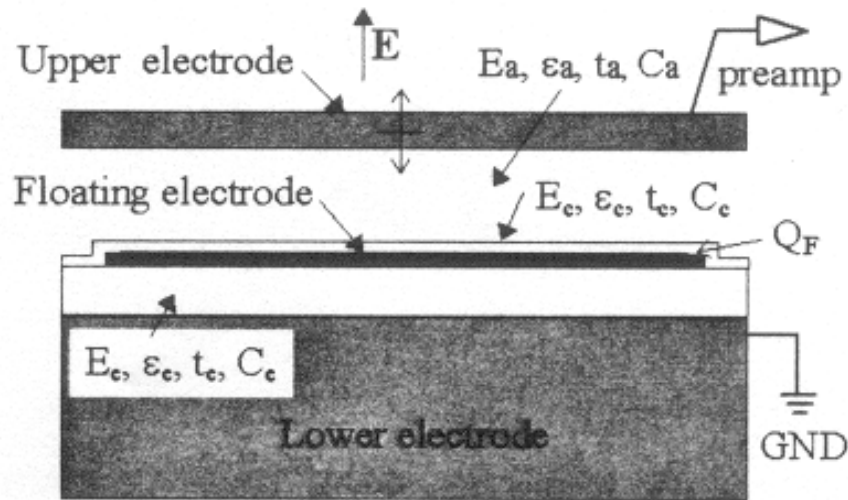


Fig. 1. Floating electrode electret configuration.

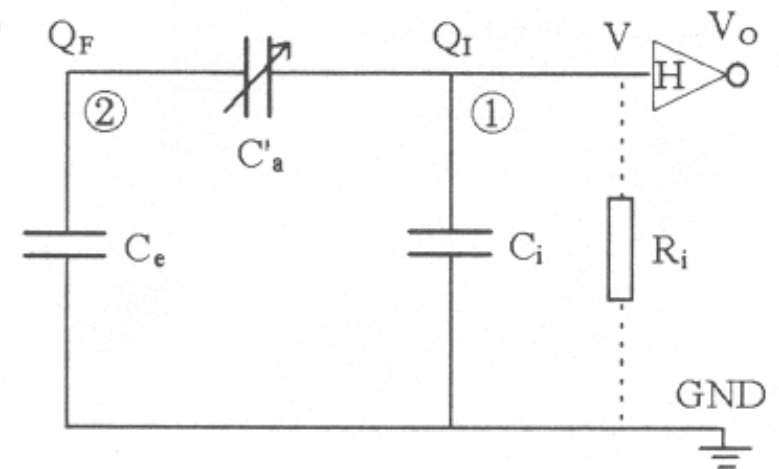
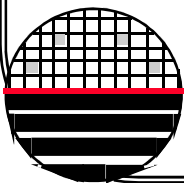


Fig. 2. Equivalent circuit of the FEEM.



ELECTRET MICROPHONE

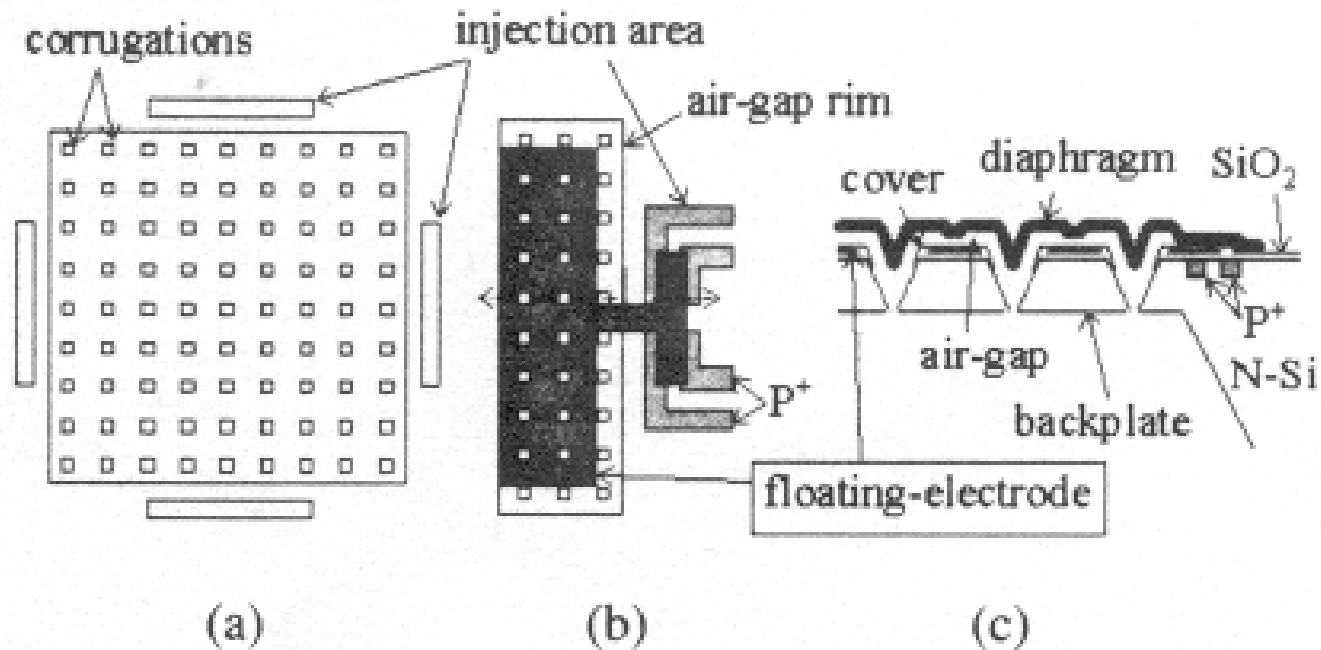
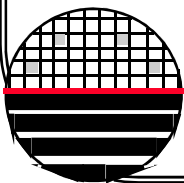


Fig. 4. (a) Microphone corrugation placement. (b) The charging and discharging configuration: top view. (c) Cross-section view.



ELECTRET MICROPHONE

4" wafers, 500 μm , (100), n-type, 2 ohm-cm, Backside polished

Deposit oxide (7000 \AA) and nitride (2000 \AA)

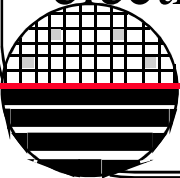
Etch from back of wafer leaving 40 μm thick silicon layer.

Fabricate JFET's for amplifier circuit.

Etch V groove corrugation from front of wafer, almost but not through the 40 μm thick silicon layer

Ion implant P+ areas for hot-electron injection charging of floating polysilicon gate

Grow 5000 \AA oxide followed by 2000 \AA polysilicon for floating electrode, dope poly, and cover with low stress silicon nitride



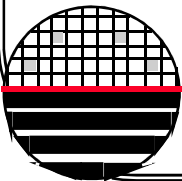
ELECTRET MICROPHONE

Next a sacrificial layer of LTO phosphosilicate glass is deposited totaling $2.7 \mu\text{m}$ in thickness

A poly layer 8000 \AA thick is deposited for the diaphragm, and doped by ion implant, followed by a 2000 \AA silicon nitride layer, a 1050 C nitrogen anneal is used to reduce stress.

Contact cuts are plasma etched and metal is deposited and patterned.

The back of the wafer is Reactive Ion Etched (RIE) to open up the V groove prior to sacrificial oxide etch in Buffered HF while the front of the wafer is protected with photoresist.



ELECTRET MICROPHONE

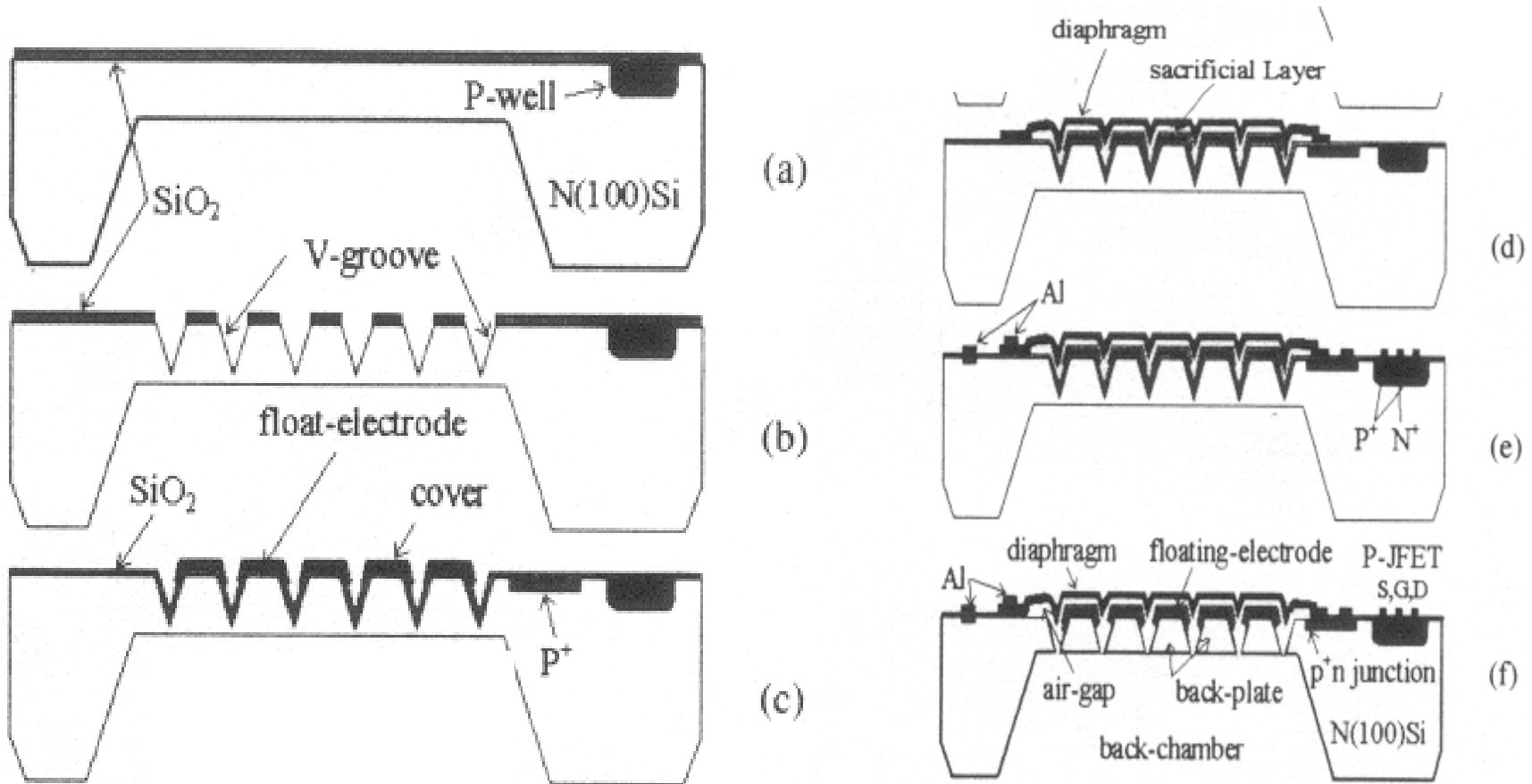
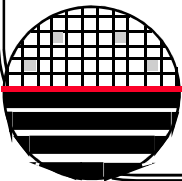
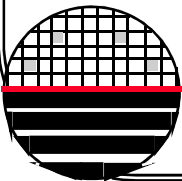
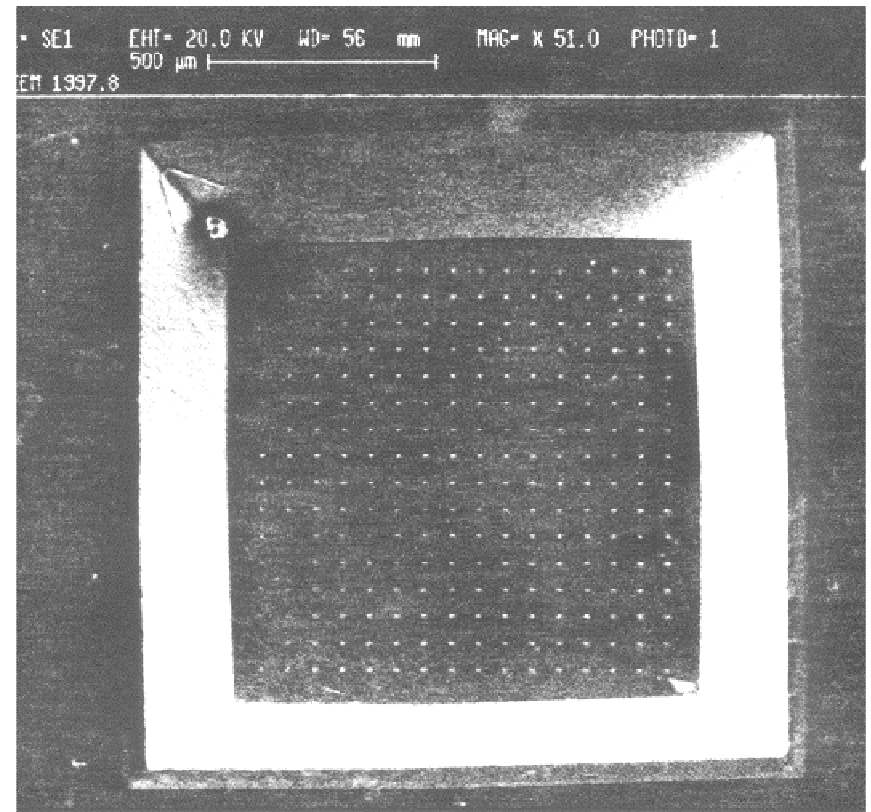
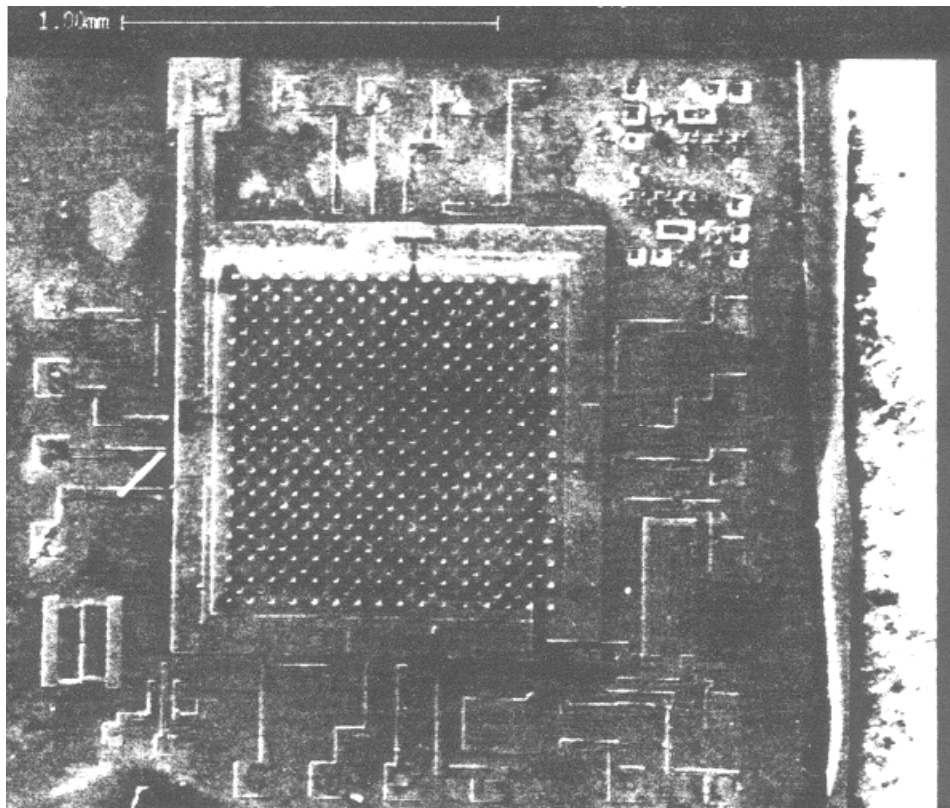


Fig. 5. Process flow of the FEEM microphone.



ELECTRET MICROPHONE



ELECTRET MICROPHONE

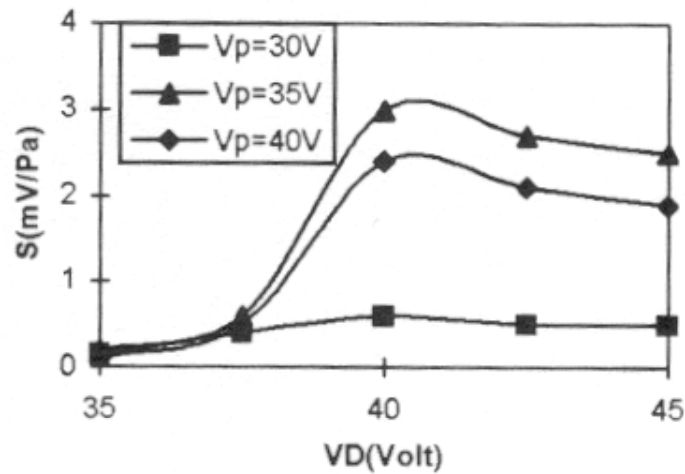


Fig. 8. Measured microphone sensitivity (S) versus V_D at different V_P .

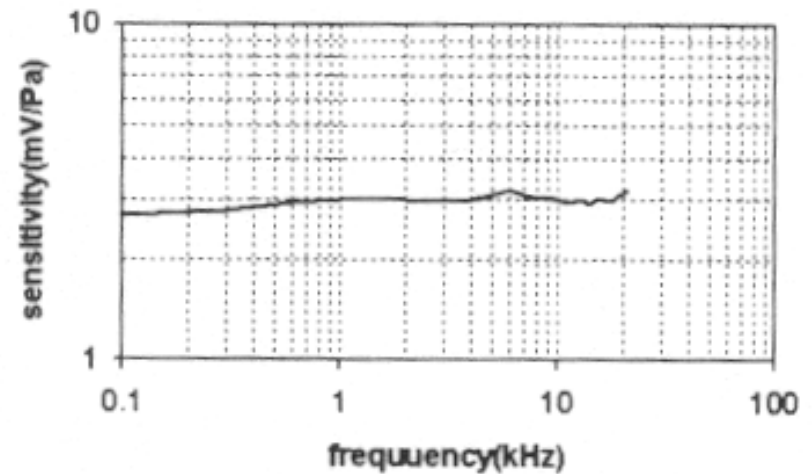
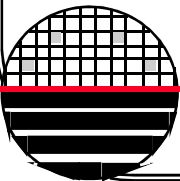


Fig. 9. Measured frequency response of the microphone.



ELECTRET MICROPHONE

Conclusion:

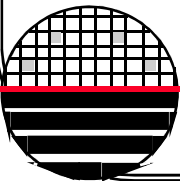
An electret integrated microphone has been proposed and developed

The charge on the floating gate is generated by hot-electron injection thus, the microphone is rechargeable, giving long life

Sensitivity of $\sim 3\text{mV/Pa}$ (measured)

Frequency response $>21\text{KHz}$ (measured)

The operation temperature can be as high as 300 C



CONDENSER MICROPHONE

JOURNAL OF MICROELECTROMECHANICAL SYSTEMS, VOL. 7, NO. 4, DECEMBER 1998

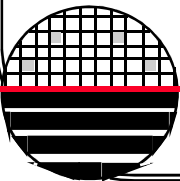
387

High-Performance Condenser Microphone with Fully Integrated CMOS Amplifier and DC–DC Voltage Converter

Michael Pedersen, Wouter Olthuis, and Piet Bergveld

Abstract—The development of a capacitive microphone with an integrated detection circuit is described. The condenser microphone is made by micromachining of polyimide on silicon. Therefore, the structure can be realized by postprocessing on substrates containing integrated circuits (IC's), independently of the IC process. Integrated microphones with excellent performances have been realized on a CMOS substrate containing dc–dc voltage converters and preamplifiers. The measured sensitivity of the integrated condenser microphone was 10 mV/Pa, and the equivalent noise level (ENL) was 27 dB(A) *re.* 20 μ Pa for a power supply voltage of 1.9 V, which was measured with no bias voltage applied to the microphone. Furthermore, a back chamber of infinite volume was used in all reported measurements and simulations. [338]

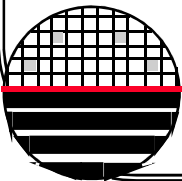
Index Terms—Capacitance transducers, integrated electronics, microphones, polyimide films, voltage multipliers.



CONDENSER MICROPHONE

Introduction

1. Fabrication is low temperature (<300 C) making this process compatible with post processing of CMOS Amplifier.
2. Both the diaphragm and the backing plate are made of polyimide coated with Cr/Pt/Cr metal and use an aluminum sacrificial layer.
3. Backside etching is done with deep trench plasma etch tool and stops on the Cr/Pt/Cr metal



CONDENSER MICROPHONE

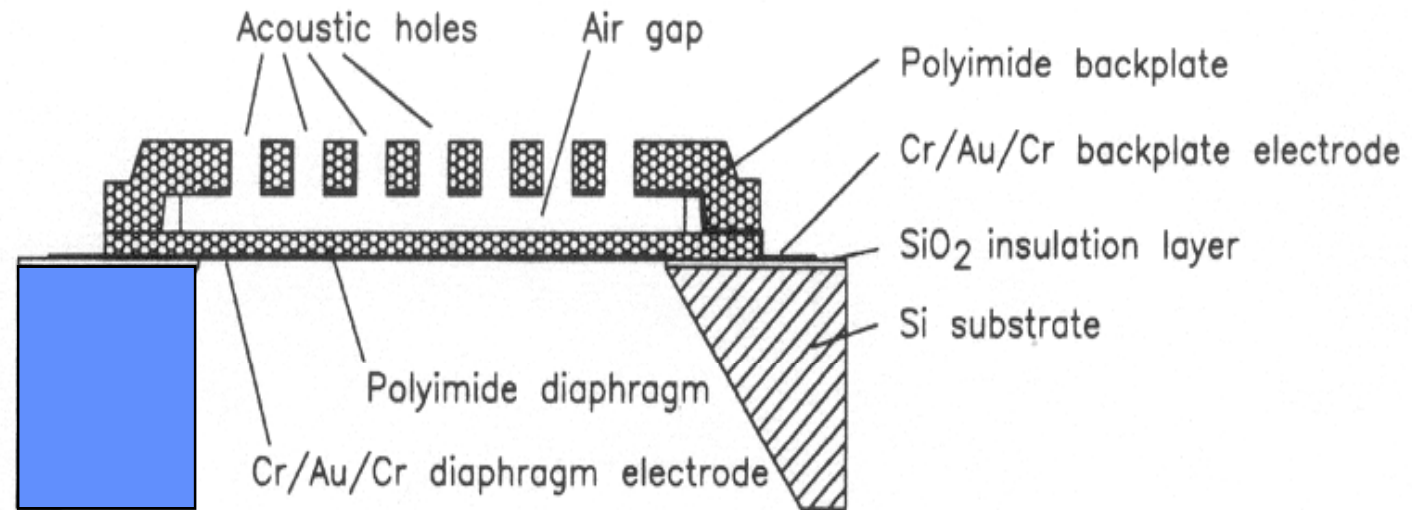
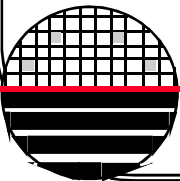
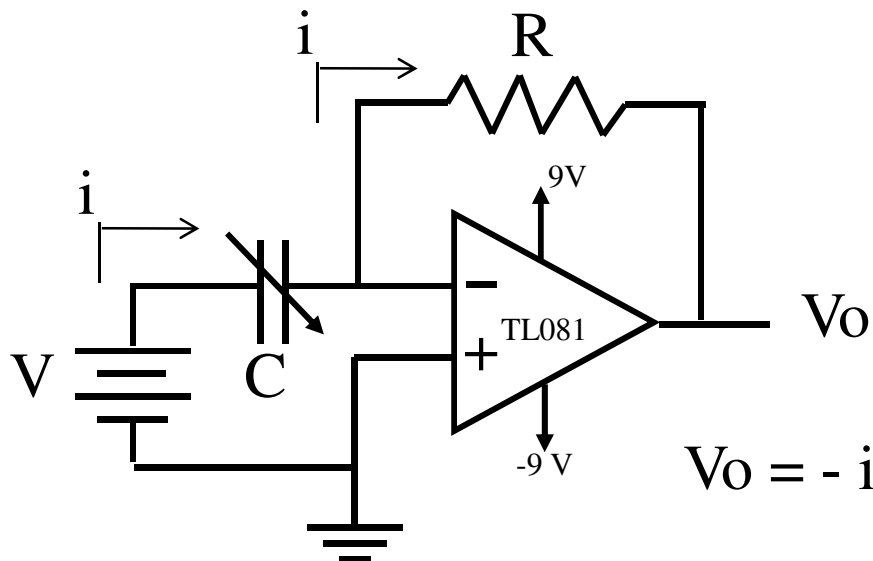


Fig. 1. Cross-sectional view of the polyimide condenser microphone.

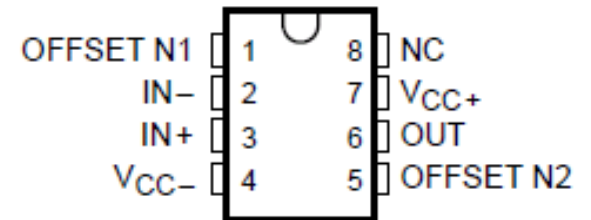
Backside hole can be etched
in KOH or with plasma
etching



SIGNAL CONDITIONING



TL081, TL081A, TL081B
D, JG, P, OR PW PACKAGE
(TOP VIEW)



$$V_o = - i R$$

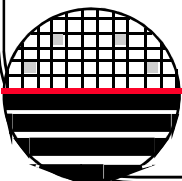
$$i = d (CV)/dt$$

$$i = V C_m 2 \pi f \cos (2\pi ft)$$

$$V_o = - \underbrace{2\pi f V R C_m}_{\text{amplitude of } V_o} \cos (2\pi ft)$$

amplitude of V_o

C_o = Average value of C
 C_m = amplitude of C change
 $C = C_o + C_m \sin (2\pi ft)$
 V is constant across C



CONDENSER MICROPHONE

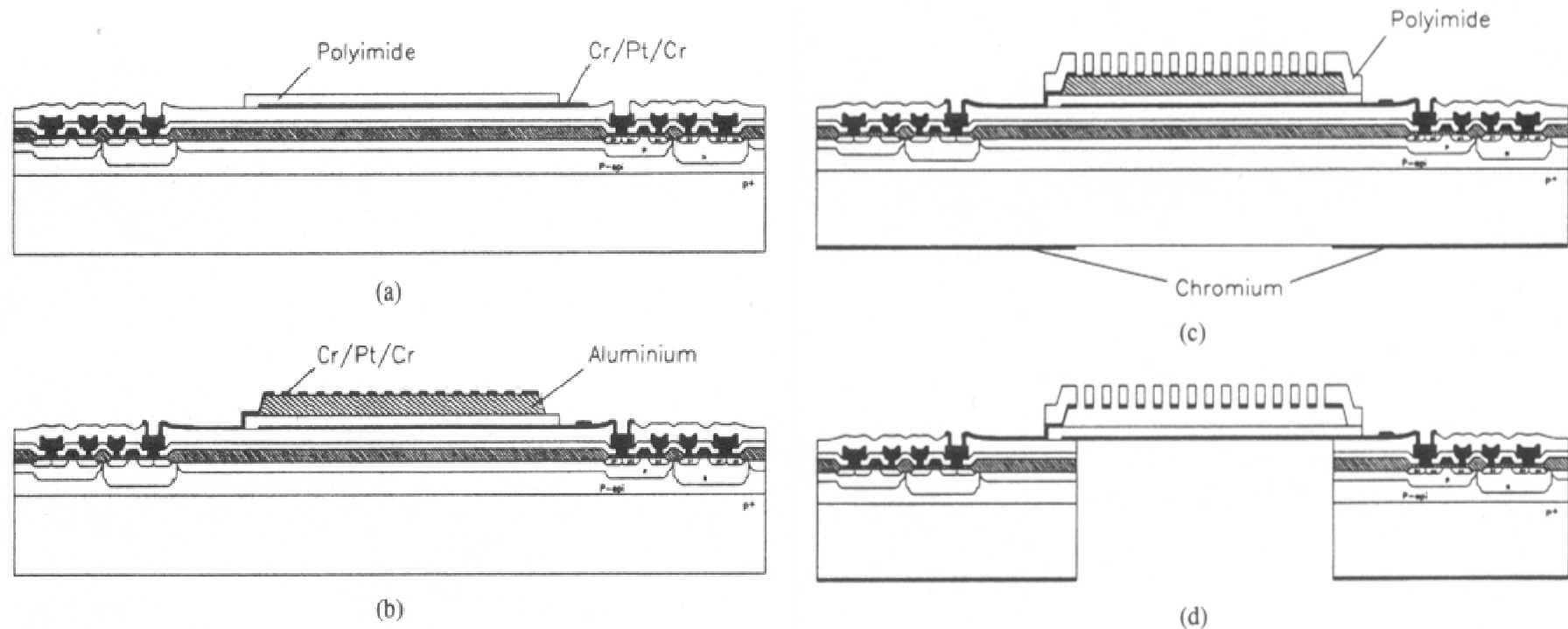
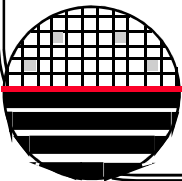


Fig. 4. Fabrication process of the integrated condenser microphone. (a) Standard CMOS processing and deposition of Cr/Pt/Cr diaphragm electrode and polyimide diaphragm. (b) Deposition of Al sacrificial layer and Cr/Pt/Cr backplate electrode. (c) Deposition of polyimide backplate and Cr etchmask on the back of substrate. (d) Etching of sacrificial layer and substrate.



CONDENSER MICROPHONE

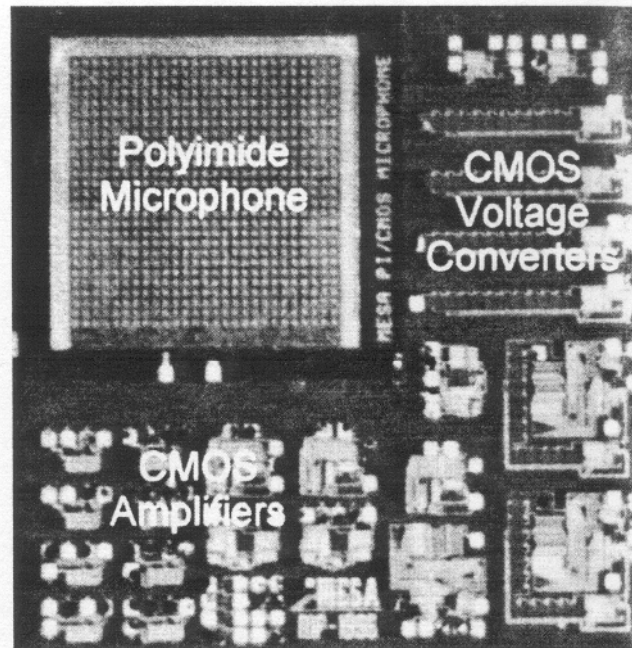
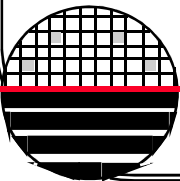


Fig. 5. Chip photograph of polyimide condenser microphone with integrated CMOS detection circuit.



CONDENSER MICROPHONE

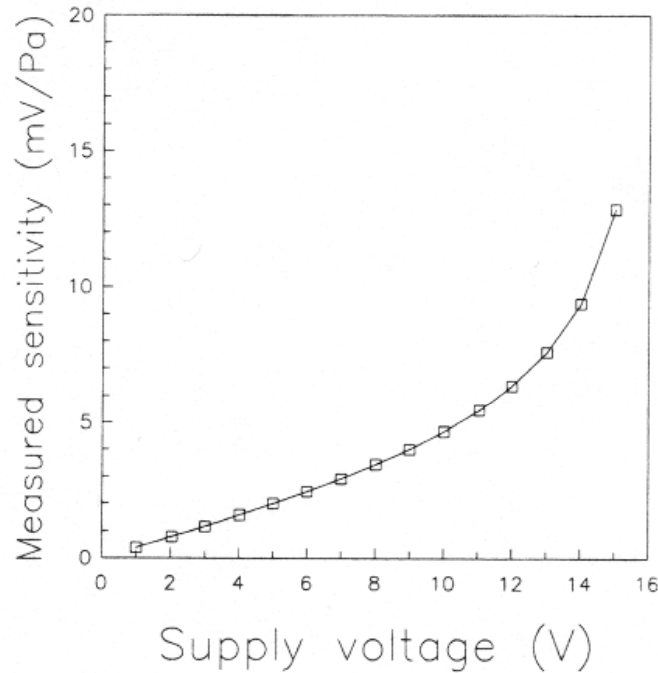


Fig. 7. Measured microphone sensitivity versus supply voltage using external biasing.

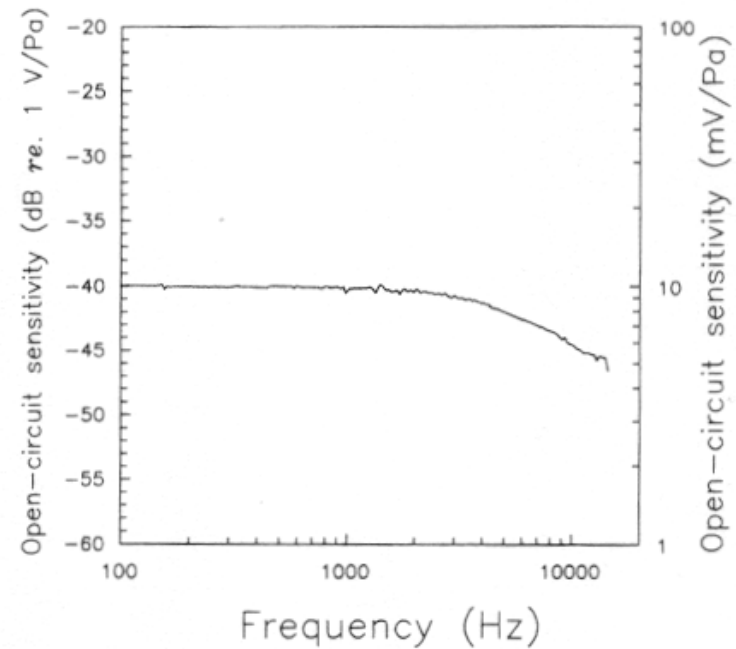
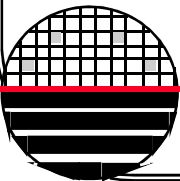


Fig. 9. Measured frequency response of the integrated microphone with a supply voltage of 1.9 V.

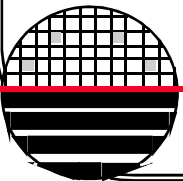


CONDENSER MICROPHONE

Conclusion:

CMOS compatible microphone process

Low temperature process



POLYSILICON DIAPHRAGM MICROPHONE

To be presented at the 1998 MEMS Conference, Heidelberg, Germany, Jan. 25-29 1998

A HIGH SENSITIVITY POLYSILICON DIAPHRAGM CONDENSER MICROPHONE

P.-C. Hsu, C. H. Mastrangelo, and K. D. Wise

Center for Integrated Sensors and Circuits

Department of Electrical Engineering and Computer Science

University of Michigan, Ann Arbor, MI 48109-2122, USA

ABSTRACT

This paper presents the analysis, design, fabrication, and testing of a condenser microphone utilizing a thin low-stress polycrystalline silicon diaphragm suspended above a p+ perforated back plate. The microphone is fabricated using a combination of surface and bulk micromachining techniques in a single wafer process without the need of wafer bonding. The device shows sensitivities of -34 dB (ref. to 1 V/Pa) for 2 mm diaphragms with bias of 13 V and -37 dB for 2.6 mm-wide diaphragms at 10 V in good agreement with expected performance calculations.

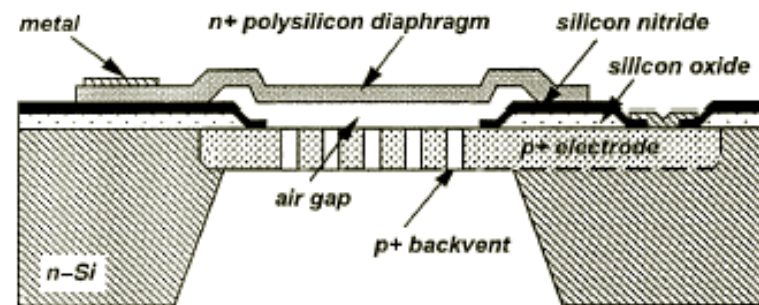


Figure 1: Cross section of the polysilicon diaphragm condenser microphone

POLYSILICON DIAPHRAGM MICROPHONE

INTRODUCTION

Many types of small-sized microphones can be constructed using silicon micromachining techniques at low cost; therefore these devices are promising for consumer electronics. Three types of silicon microphones have been developed: piezoelectric, piezoresistive, and capacitive-type [1]. Capacitive microphones show the highest sensitivity while maintaining a low power consumption. Diaphragms can be made of metal [2], p+ doped silicon [3,4], silicon nitride [5], polyimide and metal [6], and TFE [7]. The most successful devices use silicon as the diaphragm material because of its low intrinsic stress. This stress is very important because it determines the diaphragm sensitivity and its resistance to warpage. These silicon devices use a bulk micromachined p+ diaphragm with a bonded or electroplated stationary electrode.

In this paper we use low-stress polysilicon as the diaphragm electrode and a p+ etch-stop silicon plate as the back plate electrode as shown in Fig. 1. The device consists of an n-type silicon substrate, a phosphorus doped polysilicon diaphragm, a p+ perforated back plate, and the metal contacts. This arrangement permits the use of thinner diaphragms with reasonably low stress and does not require any bonding techniques.

In the sections below an electrical analog circuit is constructed to determine the microphone sensitivity. Optimal diaphragm edge width, thickness, and air gap are next determined for maximum sensitivity subject to pull-in voltage and processing constraints. Figure 2 shows a top view of a polysilicon diaphragm microphone with 2 mm diaphragm.

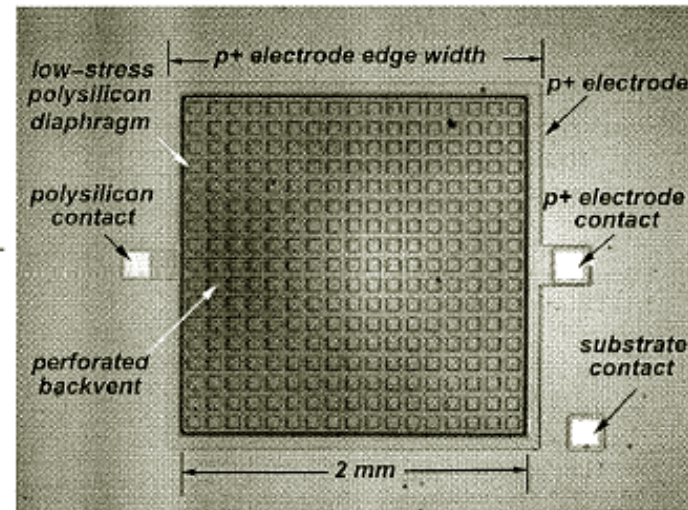


Figure 2: Top view of poly-Si diaphragm microphone

SENSITIVITY ANALYSIS

The performance of the microphone depends on the size and stress of the diaphragm. Other parameters, such as air gap distance and the bias voltage, also affect the sensitivity. The response of the capacitive microphone can be calculated using the equivalent analog electrical network of Fig. 3. The acoustic force F_{sound} and flow velocity v_m are modeled as equivalent voltage and current sources, respectively. The radiative resistance is R_r and air mass M_r . The diaphragm mechanical mass is M_m and its compliance C_m . The air gap and back vent losses are represented by viscous resistances R_g and R_h , and the air gap compliance

POLYSILICON DIAPHRAGM MICROPHONE

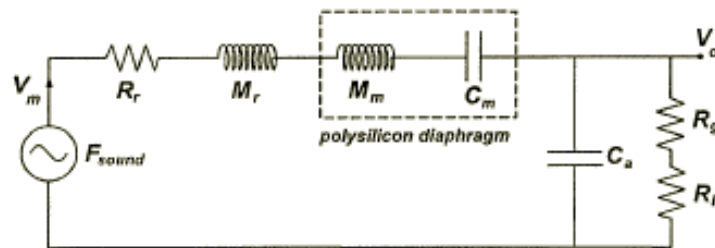


Figure 3: Equivalent electrical circuit of the condenser microphone

by C_a [4].

The diaphragm compliance depends on its flexural rigidity and tension. The flexural rigidity depends on the diaphragm thickness and the tension is determined by the polysilicon residual stress. The diaphragm deflection W can be approximated by the following differential equation:

$$-D\nabla^4 W + T\nabla^2 W = \rho \frac{\partial^2 W}{\partial \tau^2}, \quad (1)$$

where D , T , and ρ are the flexural rigidity, tensile force per unit length, and mass per unit area of the diaphragm, respectively. For the first fundamental mode, we can assume the deflection of the square diaphragm is

$$W(x, y, \tau) \approx A \sin \frac{\pi x}{a} \sin \frac{\pi y}{a} e^{-j2\pi f \tau} \quad (2)$$

where a is the diaphragm width. Substitution of Eq. (2) in Eq. (1) yields the first resonant frequency for the diaphragm

$$C_a = \frac{d}{\rho_o c^2 \alpha^2 a^2} \quad (8)$$

where n is the hole density in the backplate, α is the surface fraction occupied by the holes, u is the air viscosity coefficient, d is the average air gap distance, and ρ_o is the air density. Finally, the viscosity loss of back plate holes is approximated as [8]

$$R_h \approx \frac{8u h a^2}{\pi n r^4} \quad (9)$$

where h is the back plate height and r is the radius of hole.

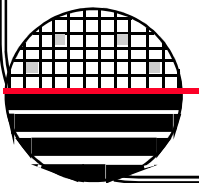
Then, the sensitivity of the microphone is the output voltage under the presence of the acoustical pressure loading, or

$$S = \frac{V_o}{P} = \frac{V_b a^2}{j\omega d Z_t} \quad (10)$$

where P is the sound pressure, V_b is the bias voltage between two electrodes, and Z_t is the total equivalent impedance of the circuit.

$$Z_t = R_r + j\omega(M_r + M_m) + \frac{1}{j\omega C_m} + \frac{R_g + R_h}{1 + j\omega(R_g + R_h)C_a} \quad (11)$$

The sensitivity of the microphone is hence a function of the frequency. A goal in our design is the maximization of sensitivity subject to fabrication and bias voltage constraints.



POLYSILICON DIAPHRAGM MICROPHONE

$$f_{res} = \sqrt{\frac{1}{\rho} \left(\frac{D\pi^2}{a^4} + \frac{T}{2a^2} \right)} \quad (3)$$

The acoustic impedance of the air in contact with the vibrating diaphragm is represented by a radiative resistance and mass. For a square diaphragm, these are approximated by [5]

$$R_r = \frac{\rho_o a^4 \omega^2}{2\pi c}, \quad M_r = \frac{8\rho_o a^3}{3\pi\sqrt{\pi}} \quad (4)$$

where ρ_o is the air density, c is the sound velocity, and ω is the angular vibration frequency ($2\pi f$).

The diaphragm compliance is equal to the average diaphragm deflection divided by the applied force. From the energy method, it is approximately

$$C_m = \frac{32a^2}{\pi^6(2\pi^2 D + a^2 T)} \quad (5)$$

The equivalent mass element M_m is derived from the kinetic energy of the square diaphragm under the uniform loading. It can be written as

$$M_m = \frac{\pi^4 \rho (2\pi^2 D + a^2 T)}{64T} \quad (6)$$

The viscosity loss in the air gap R_g and its compliance are [5, 8]

$$R_g = \frac{12ua^2}{nd^3\pi} \left(\frac{\alpha}{2} - \frac{\alpha^2}{8} - \frac{\ln \alpha}{4} - \frac{3}{8} \right) \quad (7)$$

OPTIMIZATION

Six design variables are considered: diaphragm edge width, diaphragm thickness, air gap distance, back plate thickness, hole edge width, and the surface fraction occupied by the holes. At low frequencies, the sensitivity of the microphone is approximated as

$$S_o \approx \frac{32V_b a^2}{\pi^6 T d} \quad (12)$$

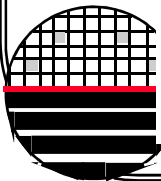
since the tension in the diaphragm dominates its compliance as the diaphragm thickness $t \rightarrow 0$. For the poly-Si diaphragm $T = \sigma_R t$ is the tensile force, and $\sigma_R \approx 20$ MPa.

The pull-in voltage for a clamped rectangular elastic plate under tension is approximately is [9]

$$V_P \approx \frac{64}{7} \sqrt{\frac{Et^3 d^3}{5(1-\nu^2)\epsilon_o a^4} \left(1 + \frac{2}{9}(1-\nu^2) \frac{\sigma_R a^2}{Et^2} \right)} \quad (13)$$

where E is the Young's modulus of the polysilicon diaphragm ($\approx 1.3 \times 10^{11}$ Pa), and ν is Poisson's ratio (≈ 0.18). From Eq. (13), the pull-in voltage is also dominated by T as $t \rightarrow 0$. If $t < 0.01a$, V_P reduces to

$$V_P \approx \frac{64}{7} \sqrt{\frac{2}{45}} \sqrt{\frac{Td^3}{\epsilon_o a^2}} \quad (14)$$



POLYSILICON DIAPHRAGM MICROPHONE

Therefore the sensitivity is related to the pull-in voltage by

$$S_o \approx \frac{\kappa}{\epsilon_o} \left(\frac{V_b}{V_P^2} \right) d^2 \quad (15)$$

where κ is a constant. For maximum sensitivity we must select the maximum gap distance d_{max} . The device capacitance must also be maximized

$$C_{mic} = \frac{\epsilon_o a^2}{d_{max}} \quad (16)$$

Therefore the maximum width a_{max} is selected. With now a and d known, the diaphragm thickness t is determined from Eq. (14)

$$t \geq \frac{2205}{8192} \frac{V_P^2 \epsilon_o a_{max}^2}{\sigma_R d_{max}^3} \quad (17)$$

Using $d_{max} = 4 \mu\text{m}$, $a_{max} = 3 \text{ mm}$, and $V_P = 12 \text{ V}$, then $t \geq 2.4 \mu\text{m}$. In our design we adopted the maximum thickness of $3 \mu\text{m}$ which satisfies all the constraints.

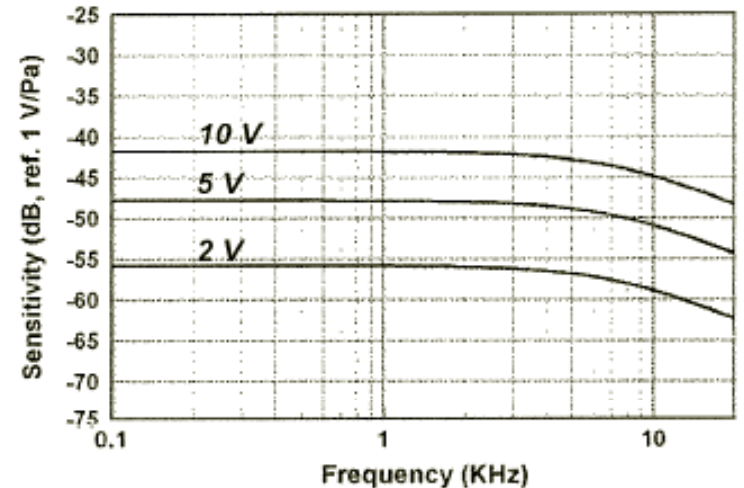
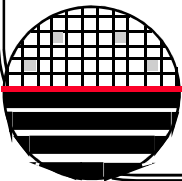


Figure 4: Calculated sensitivity frequency response for a 2.6 mm microphone

Using these values for t and d , the calculated frequency response for a 2.6 mm microphone at different biases is shown in Fig. 4. The sensitivity decays in the high frequency range due to the viscous loss in the air gap and back vent holes. The calculated resonant frequency of this device is about 25 KHz.



POLYSILICON DIAPHRAGM MICROPHONE

FABRICATION

The simplified 10-mask fabrication process of the microphone is shown in Fig. 5. On (100) *n*-type silicon wafers, a 1 μm thick wet oxide is first grown at 1100 °C for three hours. This oxide layer is patterned and etched in the buffered HF (5:1 BHF) for 12 minutes serving as a mask for the deep boron diffusion. A deep p+ boron diffusion is next introduced into the silicon from a solid source at 1175 °C for 15 hours, followed by a 20-minute wet oxidation at

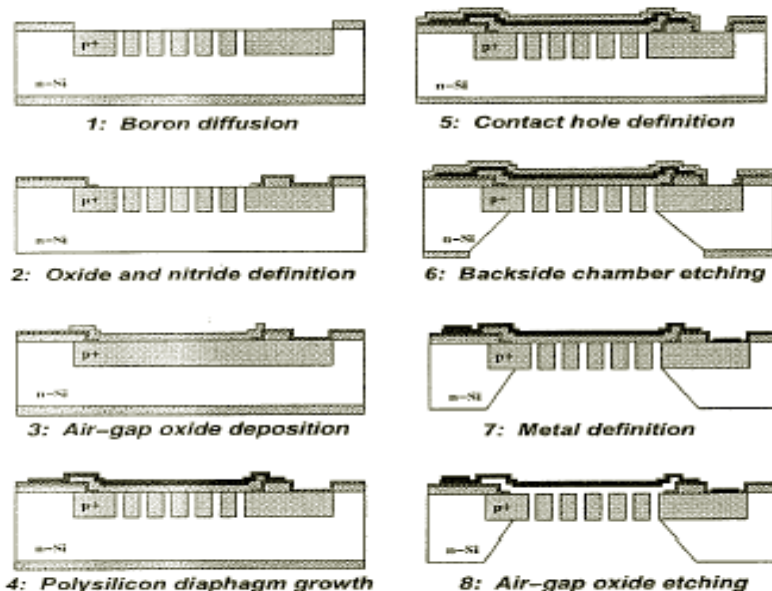


Figure 5: Simplified fabrication process of the microphone

1000 °C. The thick boron diffusion forms the stationary back electrode and the measured thickness is about 13 μm . The oxide was then stripped in a 1:1 HF:H₂O solution for 4 minutes.

A 2 μm -thick layer of LPCVD low-temperature oxide (LTO) is deposited at 420 °C for 4 hours and patterned in 5:1 BHF for 23 minutes. This oxide provides isolation for the two electrodes. A 0.3 μm -thick layer of low-stress LPCVD SiN is deposited at 875 °C. This layer is patterned and etched in hot phosphoric acid for 3 hrs. using a 0.5 μm layer of LTO as a mask. This nitride layer protects the passivation oxide from a subsequent the sacrificial etch. A 4 μm -thick LTO sacrificial layer is next deposited defining the air-gap electrode spacing. This oxide is patterned and

Next, a 2 μm -thick layer of LPCVD low-stress polysilicon is deposited at 588 °C. This material showed an unannealed tensile residual stress of about 100 MPa. The deposition is followed by a phosphorus ion implantation of $7 \times 10^{15} \text{ cm}^{-2}$ at 50 KeV. The remaining 1 μm -thick layer of polysilicon is next deposited. The polysilicon is next annealed at 1050 °C for 1 hour to redistribute the diaphragm dopants and remove as much residual stress as possible. The poly layer is next patterned and etched first using RIE with 20:5 SF₆:O₂ sccm, at 40 mT, and 60 W for 15 minutes, followed by a wet etch in 950:500:50 HNO₃:H₂O:NH₄F for 25 minutes.

A 0.6 μm -thick LTO mask is deposited and patterned in BHF for 7 min. to define the contact area of the back plate. The nitride over the contact area is then etched in hot phosphoric acid for 3 hours. A second 0.5 μm -thick LTO layer is deposited followed by a 0.2 μm Al evaporation. The LTO protects the front side of the wafer during the backside etch and the metal is used to pattern the back-to-front alignment key. The backside oxide is patterned and etched in

POLYSILICON DIAPHRAGM MICROPHONE

5:1 BHF for about 8 minutes. The wafer is then anisotropically etched in EDP for 8 hours at 110 °C. After stripping the protective LTO in 5:1 BHF for 20 min., the wafers are dried. Cr and Au are next evaporated forming the contact pads with thickness of 50 and 400 nm. The metal is next patterned and wet Au and Cr etchants for 4 and 1 min, respectively.

Finally, the device is released in concentrated HF for 1 hour. In this operation, the HF removes the sacrificial LTO from the backside while the wafer front is protected by the SiN layer. After rinsing the samples thoroughly, the chips are diced and wire bonded to a DIL metal package.

Figures 6-9 shows SEM pictures of the fabricated microphone. Figure 6 shows the top view of a $2.6 \times 2.6 \text{ mm}^2$ device. Contacts for both polysilicon diaphragm and back plate are at opposing sides of the device. Figure 7 shows a close up view of the polysilicon diaphragm edge. The p+ back plate is made slightly larger than the diaphragm to account for misalignments and uncertainties on the wafer thickness during the back side etch. The shallow squares of the back-plate holes are visible at the front of the diaphragm due to the oxide step created during the deep boron diffusion. Figure 8 shows microphone backside. The back plane shows the periodic $60 \times 60 \text{ }\mu\text{m}^2$ hole array that provide a back vent for the polysilicon diaphragm. Figure 9 shows a close up of the back plate holes after the sacrificial oxide etch. The $4 \text{ }\mu\text{m}$ air gap is clearly visible. The curvature of the holes is a result of the deep boron diffusion. The p+ back plate is $13 \text{ }\mu\text{m}$ -thick.

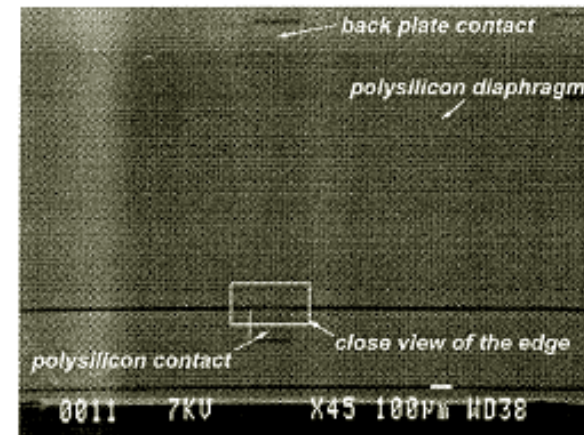


Figure 6: Top view of the microphone

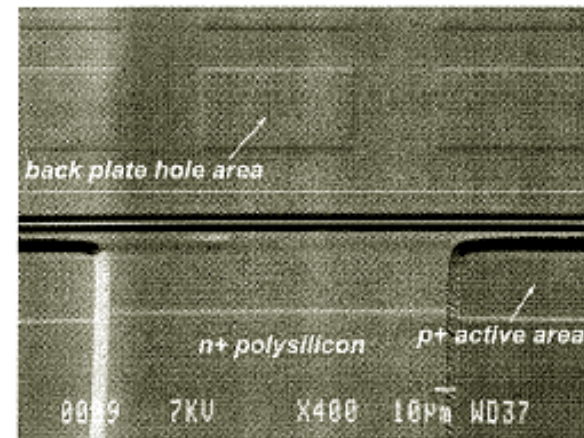


Figure 7: Closeup view of the diaphragm edge

POLYSILICON DIAPHRAGM MICROPHONE

MEASUREMENTS

The capacitance of the microphone was measured as a function of the applied bias using an HP 4284A precision LCR meter. Figure 10 shows the measured capacitance versus bias voltage of the microphone with a 2.6 mm diaphragm. At zero bias the microphone exhibits a 16.2 pF capacitance in close agreement to the calculated result. The capacitance increases as the bias voltage increases. The pull-in voltage is about 10 V.

In order to test the sensitivity of the microphone, the device was placed in the sound isolation box shown Fig. 11. The interior of the box is covered with SONEX prospec polyurethane composite foam providing a barrier to external noise and internal sound absorption. The microphone is driven with a speaker connected to a HP33120A waveform generator. The condenser or reference microphone is connected to a preamplifier which converts the capacitor variation to the voltage output. A calibrated ACOJ7012 free-field microphone is used as the reference microphone. Both microphones are connected to an HP ACOP4012 preamplifier with a internal impedance of 2.5 G Ω . The preamplifier is connected an HP ACOP9200 microphone power supply which provides an internal DC polarization voltage of 200 V for the reference microphone. For the device condenser microphone, the bias voltage is adjusted externally. The output voltage is recorded using an HP3561A dynamical signal analyzer.

Figure 7: Closeup view of the diaphragm edge

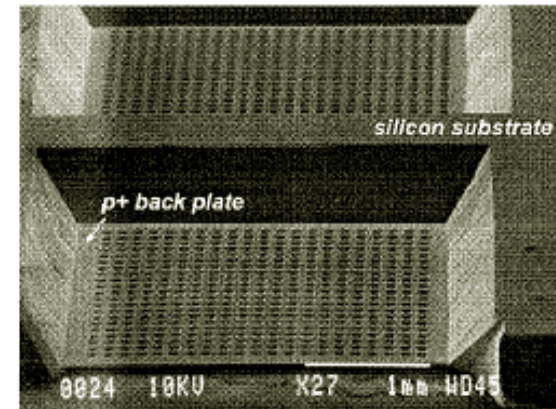


Figure 8: Back view of the microphone

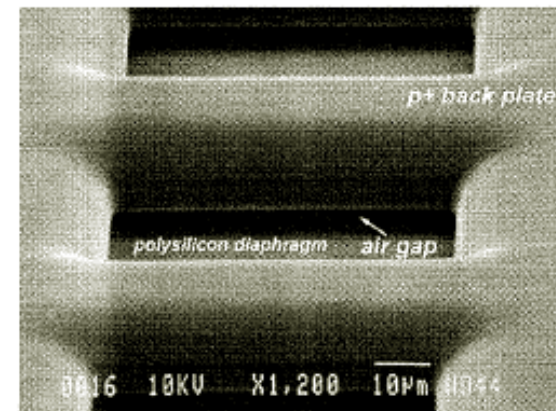
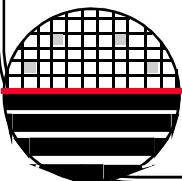


Figure 9: Closeup view of the back plate holes



POLYSILICON DIAPHRAGM MICROPHONE

The measurement starts with the calibration of the reference microphone using a HP ACOP511E calibrator, which exhibits a standard sound level of 1 Pa at 1 KHz. The characteristics of the speaker are next determined using the reference microphone. Next the reference microphone is replaced by the condenser microphone and the bias voltage is adjusted to a desired level. The sensitivity of the microphone is obtained by subtracting the reference response from the device response plus the calibration output level.

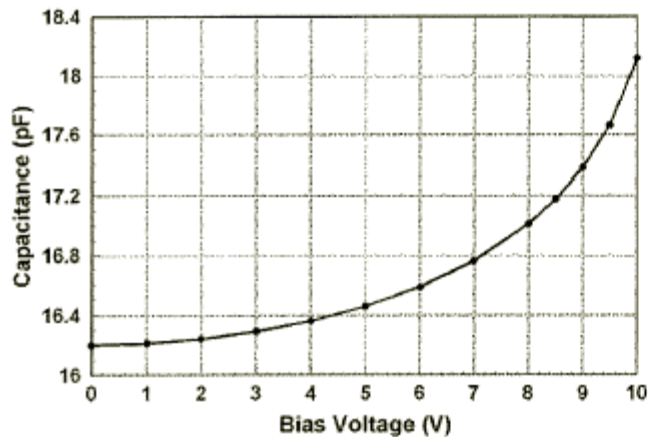


Figure 10: Measured capacitance versus bias voltage of a 2.6-mm wide microphone

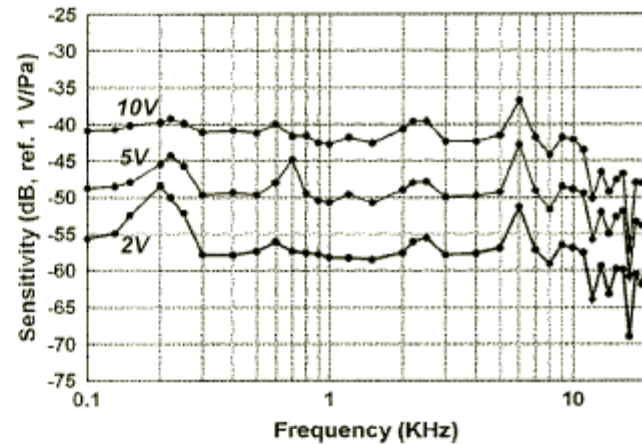
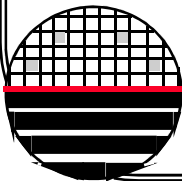
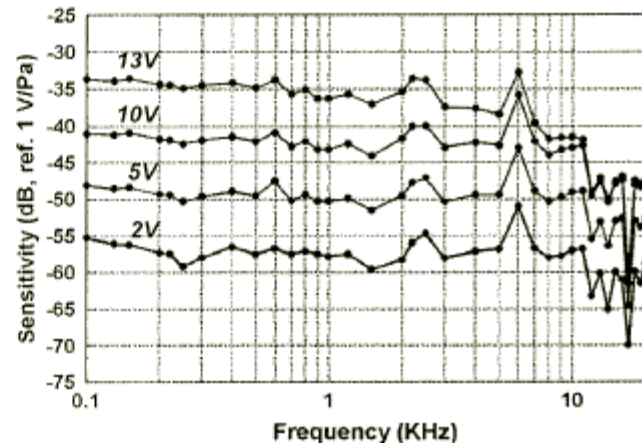


Figure 12: Experimental frequency response of a 2.6 mm microphone



POLYSILICON DIAPHRAGM MICROPHONE

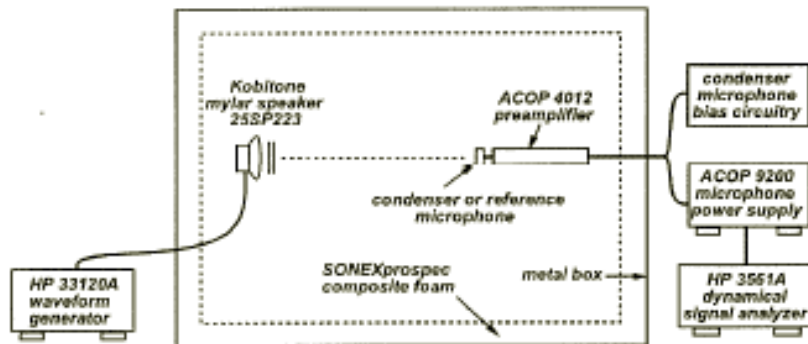


Figure 11: Block diagram of the microphone measurement setup

Figure 12 shows the frequency response of a 2.6 mm-wide microphone at three different bias voltages. With a bias voltage of 10 V, the microphone exhibits a sensitivity between -44 and -36 dB from DC to 10 KHz. The sensitivity decreases 5 to 8 dB when using a 5 V bias. These measurements are in close agreement with the calculated values of Fig. 4 with a residual stress of 20 MPa.

Figures 13-14 show the highest sensitivity achieved for diaphragm widths of 2 and 3 mm. With a bias voltage of 13 V, the 2 mm-wide microphone has a sensitivity between -32 and -42 dB. The 3 mm-wide microphone shows a high sensitivity between -37 and -47 dB for a bias voltage of 9 V.

Figure 13: Frequency response of a 2 mm microphone

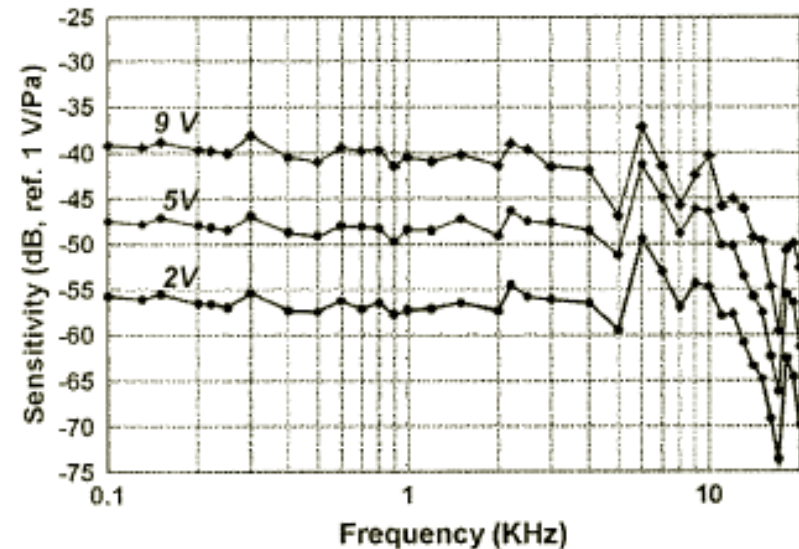
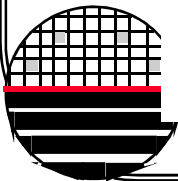


Figure 14: Frequency response of a 3 mm microphone



POLYSILICON DIAPHRAGM MICROPHONE

SUMMARY

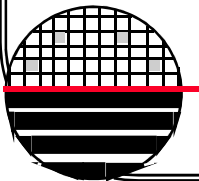
This paper presents the design and fabrication of condenser microphone using a low-stress polysilicon diaphragm suspended above a p+ perforated back plate. The microphone performance matches expected calculated values yielding a sensitivity of about -34 dB. The microphone dimension is optimally designed to achieve the highest sensitivity. The device is fabricated using a single wafer process without need of wafer bonding.

ACKNOWLEDGEMENTS

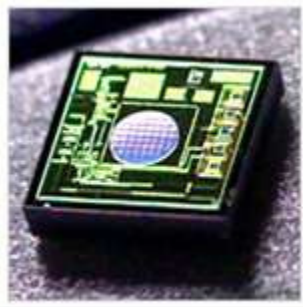
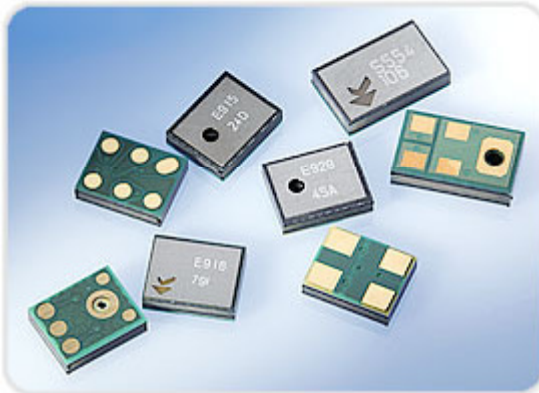
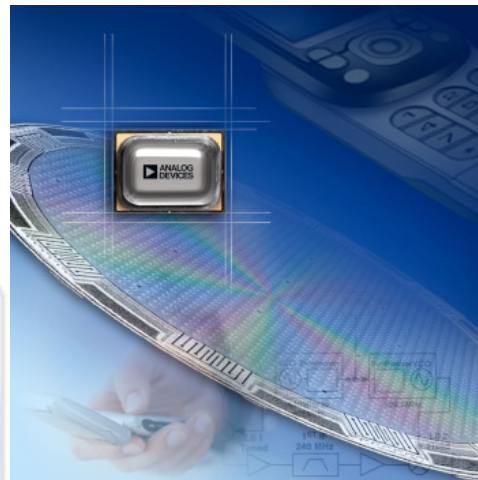
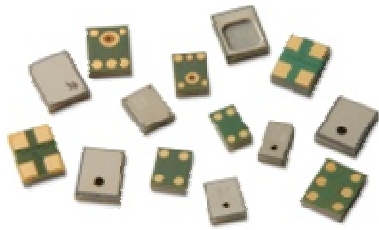
This work was supported by the Defense Advanced Research Projects Agency (DARPA) under contract DABT63-C-0111. We thank the staff and graduate students of the UM Center for Integrated Sensors and Circuits for their helpful assistance during the device fabrication.

References

- [1] P. R. Scheeper, A. G. H. van der Donk, W. Olthuis, and P. Bergveld, "A review of silicon microphones," *Sensors and Actuators A*, vol. 44, pp. 1–11, 1994.
- [2] J. A. Voorthuyzen, P. Bergveld, and A. J. Sprenkels, "Semiconductor-based electret sensors for sound and pressure," *IEEE Trans. on Electrical Insulation*, vol. 24, pp. 267–276, April 1989.
- [3] J. J. Bernstein and J. T. Borenstein, "A micromachined silicon condenser microphone with on-chip amplifier," *Solid-State Sensor and Actuator Workshop*, pp. 239–243, 1996.
- [4] J. Bergqvist and F. Rudolf, "A silicon condenser microphone using bond and etch-back technology," *Sensors and Actuators A*, vol. 45, pp. 115–124, 1994.
- [5] W. Kuhnel and G. Hess, "A silicon condenser microphone with structured back plate and silicon nitride membrane," *Sensors and Actuators A*, vol. 30, pp. 251–258, 1992.
- [6] M. Pedersen, W. Olthuis, and P. Bergveld, "A polymer condenser microphone on silicon with on-chip CMOS amplifier," *1997 Int. Conf. Solid-State Sensors and Actuators (Transducers 97)*, pp. 445–446, 1997.
- [7] W. H. Hsieh, T.-Y. Hsu, and Y.-C. Tai, "A micromachined thin-film teflon electret microphone," *1997 Int. Conf. Solid-State Sensors and Actuators (Transducers 97)*, pp. 425–428, 1997.
- [8] J. Bergqvist, "Finite-element modelling and characterization of a silicon condenser microphone with a highly perforated backplate," *Sensors and Actuators A*, vol. 39, pp. 191–200, 1993.
- [9] C. H. Mastrangelo, "Adhesion-related failure mechanisms in micromechanical devices," *Tribology Letters*, pp. 223–237, 1997.



COMMERCIAL MICROPHONES



Akustica
Analog Devices
Boesch
Emkay Sisonic
Futurlec
Infineon
Knowles
Motorola
STMicroelectronics
TI
Others

*Rochester Institute of Technology
Microelectronic Engineering*

AKU1126 MICROPHONES

AKUSTICA

Datasheet

September 2009

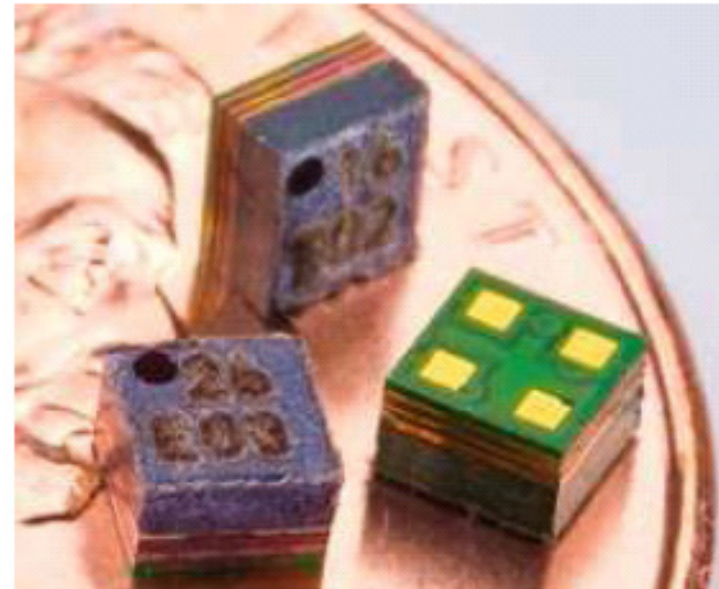
AKU1126 Single-Chip Analog Microphone

GENERAL DESCRIPTION

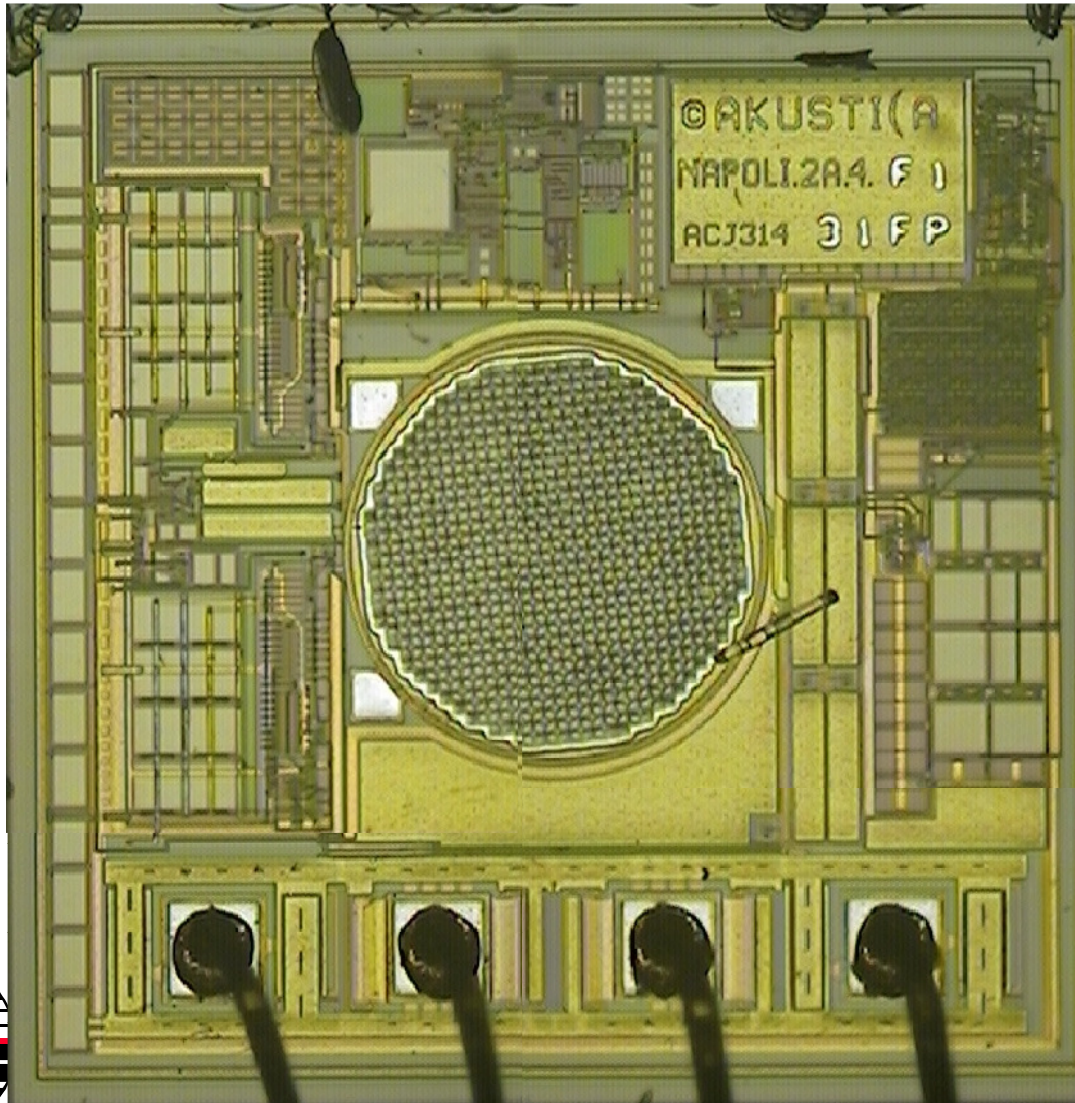
The AKU1126 is the world's smallest, analog-output microphone that uses standard semiconductor packaging technology and materials. While other microphones degrade in performance as they shrink in size, the AKU1126 maintains superior performance in an ultra-small form factor.

The AKU1126's gain select feature, accessed by use of a single external resistor, allows the microphone to be used in both near-ear applications as well as far-field applications - such as speaker phones or headsets - without the use of additional amplifiers.

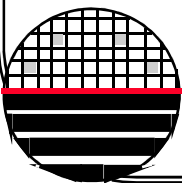
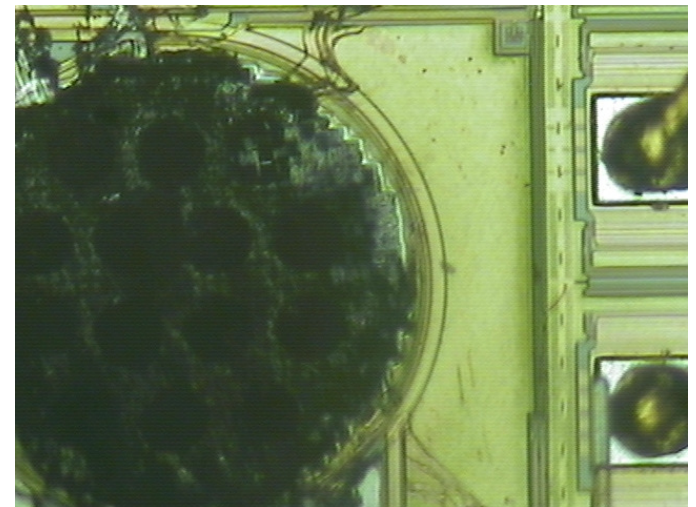
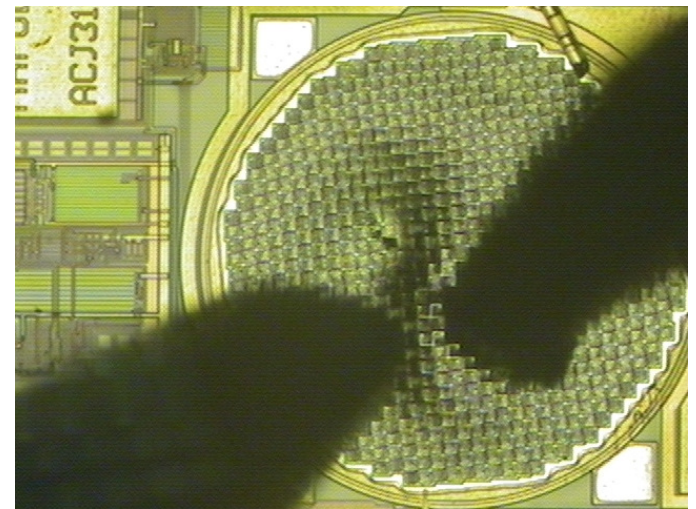
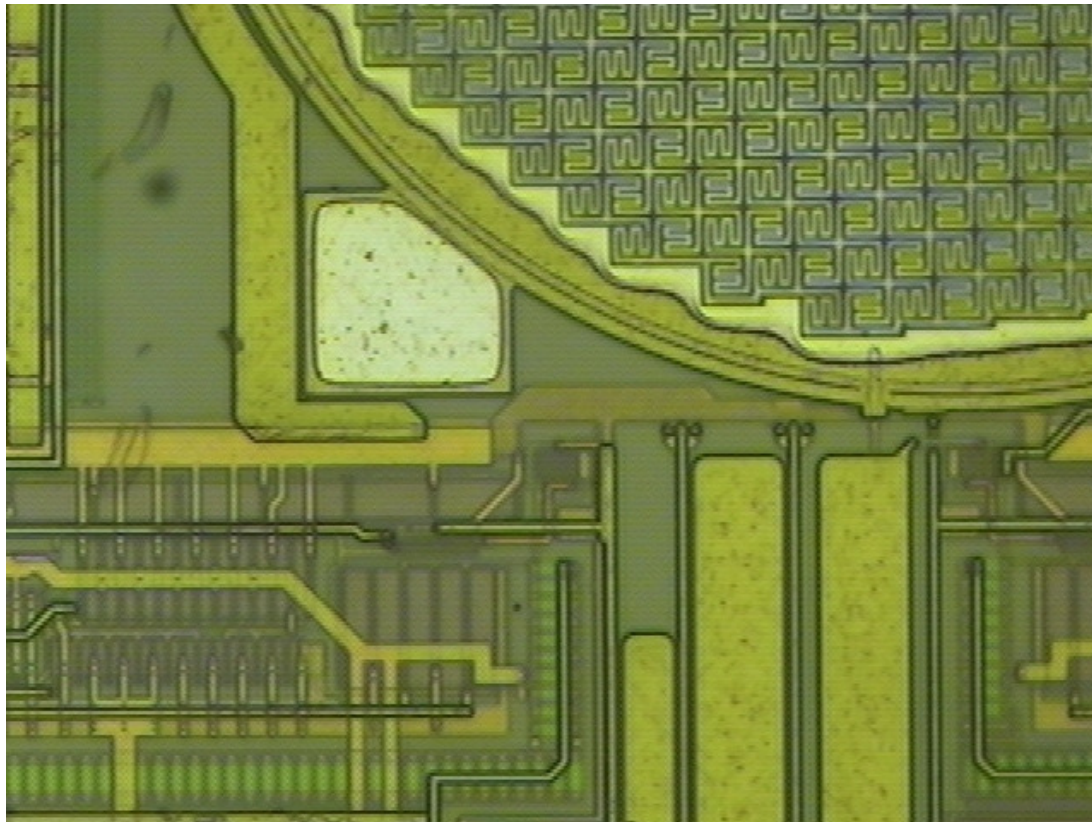
The AKU1126 is the first microphone product to leverage Akustica's 1mm x 1mm CMOS MEMS microphone die – a monolithic solution which integrates the acoustic transducer and accompanying electronics in a single chip of silicon. In contrast to other silicon microphones, Akustica's one die approach eliminates the need for inter-die wirebonds, allowing for smaller, higher performance, more reliable products.



AKU1126 MICROPHONE

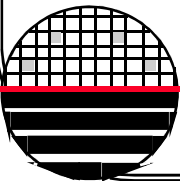


AKU1126 MICROPHONE



REFERENCES

1. “Microsensors,” Muller, Howe, Senturia, Smith and White, IEEE Press, NY, NY 1991.
2. “Sensor Technology and Devices,” Ristic, L.J., Artech House, London, 1994
3. Journal of Microelectromechanical Systems, IEEE



HW – MICROPHONES

1. Find another publication describing the fabrication of a MEMs pressure sensor (or microphone). Describe the fabrication sequence in your own words. Attach a copy of the paper.
2. What is the difference between a condenser microphone and an electret microphone?
3. Why are there holes in the backing plate in a MEMS microphone?

